Inorganic Chemistry

Article

pubs.acs.org/IC

Hydroxamate Anchors for Improved Photoconversion in Dye-Sensitized Solar Cells

Timothy P. Brewster,[†] Steven J. Konezny,* Stafford W. Sheehan, Lauren A. Martini, Charles A. Schmuttenmaer,* Victor S. Batista,* and Robert H. Crabtree*

Department of Chemistry, Yale University, P.O. Box 208107, New Haven, Connecticut 06520-8107, United States

Energy Sciences Institute, Yale University, P.O. Box 27394, West Haven, Connecticut 06516-7394, United States

Supporting Information

ABSTRACT: We present the first analysis of performance of hydroxamate linkers as compared to carboxylate and phosphonate groups when anchoring ruthenium-polypyridyl dyes to TiO_2 surfaces in dye-sensitized solar cells (DSSCs). The study provides fundamental insight into structure/function relationships that are critical for cell performance. Our DSSCs have been produced by using newly synthesized dye molecules and characterized by combining measurements and simulations of experimental current density−voltage (*J-V*) characteristic curves. We show that the choice of anchoring group has a direct effect on the overall sunlight-to-electricity conversion efficiency (η), with hydroxamate anchors showing the best performance. Solar cells based on the pyridyl-hydroxamate complex exhibit higher efficiency since they suppress electron transfer from the photoanode to the electrolyte and have superior photoinjection characteristics. These findings suggest that hydroxamate anchoring groups should be particularly valuable in DSSCs and photocatalytic applications based on molecular adsorbates covalently bound to semiconductor surfaces. In contrast, analogous acetylacetonate anchors might undergo decomposition under similar conditions suggesting limited potential in future applications.

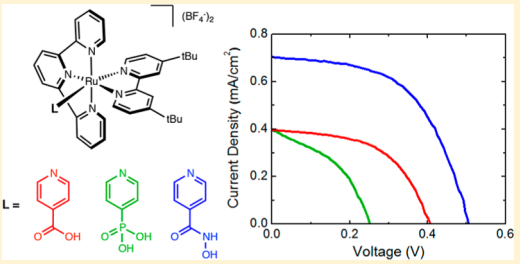

INTRODUCTION

The efficient utilization of solar energy is a promising solution to current energy and environmental concerns.[1] Traditional photovoltaic devices, however, are based on costly p-n junctions of high-quality silicon wafers, making solar cells affordable only at a moderate scale, or for specific applications (e.g., satellites).[2,3] Therefore, there has been significant interest in the development of alternative solar cells based on inexpensive materials such as dye-sensitized solar cells (DSSCs) made of sensitized nanoparticulate thin-films.[4] Since the work by O'Regan and Grätzel in 1991,[5] DSSCs quickly reached conversion efficiencies >10%.[6] However, only modest improvements in efficiency have been reported over the last 20 years since these initial breakthroughs.[7−9] This has been partially due to the lack of understanding of how the various redox/transport processes determine the overall cell performance and how they are affected by the nature of the assembly components. In this article, we focus on the effect of anchoring groups on the overall sunlight-to-electricity conversion. To the best of our knowledge, this is the first analysis of performance of hydroxamate linkers as compared to carboxylate and phosphonate groups when anchoring ruthenium-polypyridyl dyes to TiO_2 surfaces, in complete dye-sensitized solar cells (DSSCs).

Figure 1 shows a schematic diagram of a DSSC, including the photoexcitation, redox, and transport processes initiated by absorption of visible light. While the TiO_2 band gap lies in the UV region (at approximately 3.0−3.2 eV),[10] functionalization of TiO_2 surfaces with dye molecules sensitizes them to absorption of visible light. Electrons are transferred to the conduction band of the semiconductor upon photoexcitation of a dye to an excited electronic state that is isoenergetic with electronic states in the TiO_2 conduction band. The injected electron can flow through an external circuit and be collected by the counter-electrode. A redox mediator, most commonly I_3^-/I^-, then accepts the electron from the cathode and fills the hole left on the dye.[4] Important aspects for optimization of the cell performance are, thus, selection of the dye and its attachment motif to the semiconductor surface.

Many of the most efficient DSSC dyes are ruthenium-polypyridyl complexes.[6,7,11−13] Small variations in the dye structure can lead to large changes in the overall cell performance.[7,14] Ligand exchange affects the visible absorption, and thus the overall efficiency, of $Ru(dcbpy)_2X_2$ (dcbpy = 2,2′-bipyridyl-4,4′-dicarboxylate, X = Cl^-, Br^-, I^-, CN^-, SCN^-) with the thiocyanate complex giving the best performance.[6] Other important changes that can dramatically affect solar cell efficiency are the protonation state of the carboxylate anchoring groups in $Ru(dcbpy)_2(NCS)_2$[13] and modifications of the pyridyl-based ligands.[9] Impressively, $Ru(dcbpy)_2(NCS)_2$, and other analogous complexes have been shown to have incident photon to charge carrier conversion efficiencies of unity across portions of the visible spectrum.[6,7,12,13]

Received: May 1, 2013
Published: May 21, 2013

   dx.doi.org/10.1021/ic4010856 | *Inorg. Chem.* 2013, 52, 6752−6764

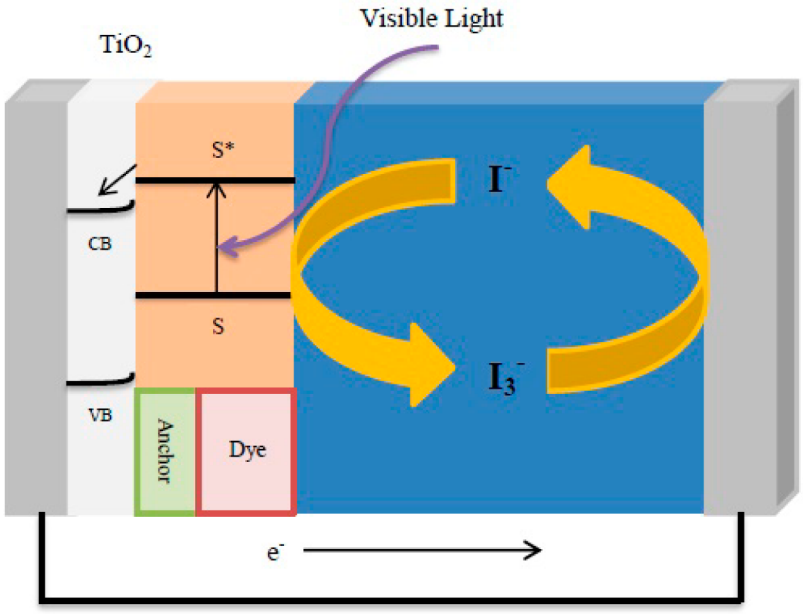

Figure 1. Schematic representation of a dye-sensitized solar cell.

Though effective in DSSCs, dyes bearing carboxylate anchors have been shown to have limited stability in aqueous and highly oxidizing conditions.[15,16] This would make them unsuitable for use in an artificial photosynthetic cell. In such a device the redox mediator is removed and the acetonitrile solvent is replaced by water. The circuit is then closed by oxidation of water to dioxygen at the anode and cathodic reduction of the generated protons to dihydrogen.[10,17] A few examples of functional water-splitting cells based on such scheme have been reported,[18−22] showing promise of a viable way of capturing and storing solar energy.

Many water stable anchoring groups have been suggested as replacements for carboxylates in DSSC and artificial photosynthesis applications. Phosphonate anchors are the most commonly implemented,[15,16,23,24] although hydroxamate,[25−27] catecholate,[28,29] and acetylacetonate[30−33] anchors have also been explored. To date, however, most reported water-splitting devices based on molecular catalysts have employed phosphonates to anchor the dye molecules to TiO_2 thin-films.[21,22]

Phosphonate anchors bind to TiO_2 surfaces more tightly than carboxylates.[16] However, they are usually less efficient than carboxylates at facilitating interfacial electron transfer.[34,35] The reduced electron injection efficiency is not always a problem since some phosphonate complexes are capable of quantitative electron injection.[36] Additionally, the decrease in injection rate does not always correlate with a decrease in photoconversion efficiency. In fact, there are examples of systems in which ruthenium dyes bound through phosphonic acid anchors outperform their carboxylate counterparts because of differential rates of other charge transfer processes required for cell operation.[24,37] Recently, an attempt to combine the binding affinity of the phosphonate anchor with the electron injection efficiency of carboxylates was reported.[38] Though this method proved successful for the reported sensitizer, applications may be limited because of the geometric constraints imposed by this strategy.

In contrast to phosphonates, hydroxamates have been shown to bind more tightly to semiconductor surfaces *and* inject electrons into TiO_2 more efficiently than the industry-standard carboxylates, thus resolving both issues with a single anchor.[25,39] These advantages are presumably due to dianionic character. Specifically, hydroxamic acids, R-CONHOH, can undergo facile double deprotonation, thus providing dianionic anchoring groups that readily form oxidation- and water-stable 5-membered chelate rings with suitable metal ions (eq 1). In this way,

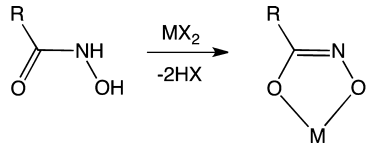

(1)

hydroxamic acids find use in both pharmacological and bioinorganic applications, acting as metal-binding groups in drugs and siderophores, respectively.[40] While ruthenium complexes with acetylacetonate anchors have been studied,[33] ruthenium complexes bearing hydroxamate anchors have not been investigated for solar applications, probably because of the lack of previously established synthetic pathways. Additionally, the direct effect of the hydroxamate anchor on sunlight-to-electricity conversion efficiency has not been previously investigated. In fact, to the best of our knowledge, no DSSC data has been previously reported for a dye bearing a hydroxamate anchor.

This paper focuses on the synthesis of ruthenium dyes that differ only in their anchoring group and the analysis of their performance in DSSCs. We analyze our own series of new dyes of the form $[Ru(terpy)(tbbpy)L][BF_4]_2$ (terpy = 2,2′;6′,2″-terpyridine, tbbpy = 4,4′-di-*tert*-butyl-2,2′-bipyridine, L = anchoring ligand), that have been synthesized, characterized spectroscopically, and tested for their efficiency in complete DSSC assemblies. Their relative performance is assessed through measurements of the current−voltage (*J-V*) characteristic curves and simulations of the *J-V* curves based on an equivalent circuit model, as in previous work.[41] The analysis shows how different anchoring groups affect photoconversion efficiency by changing the various current components, including photoinjection, recombination, and the shunt current. Hydroxamate complexes

dx.doi.org/10.1021/ic4010856 | *Inorg. Chem.* 2013, 52, 6752−6764

Scheme 1. Synthesis of [Ru(terpy)(tbbpy)(pyr-COOH)][BF_4]$_2$ (3)

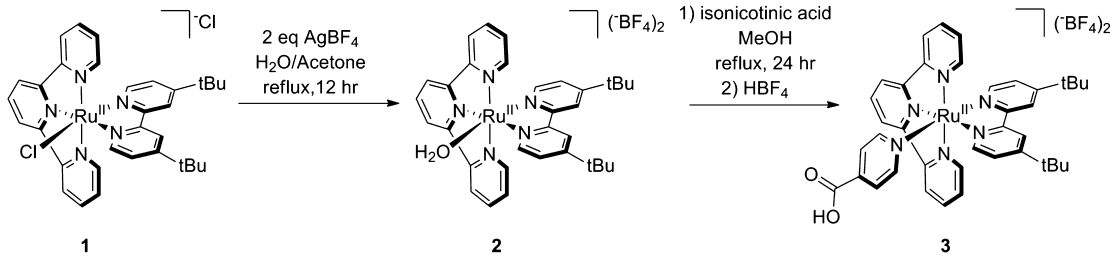

Scheme 2. Synthesis of [Ru(terpy)(tbbpy)(pyr-hydrox)][BF_4]$_2$ (4) and [Ru(terpy)(tbbpy)(pyr-phos)][BF_4]$_2$ (6)

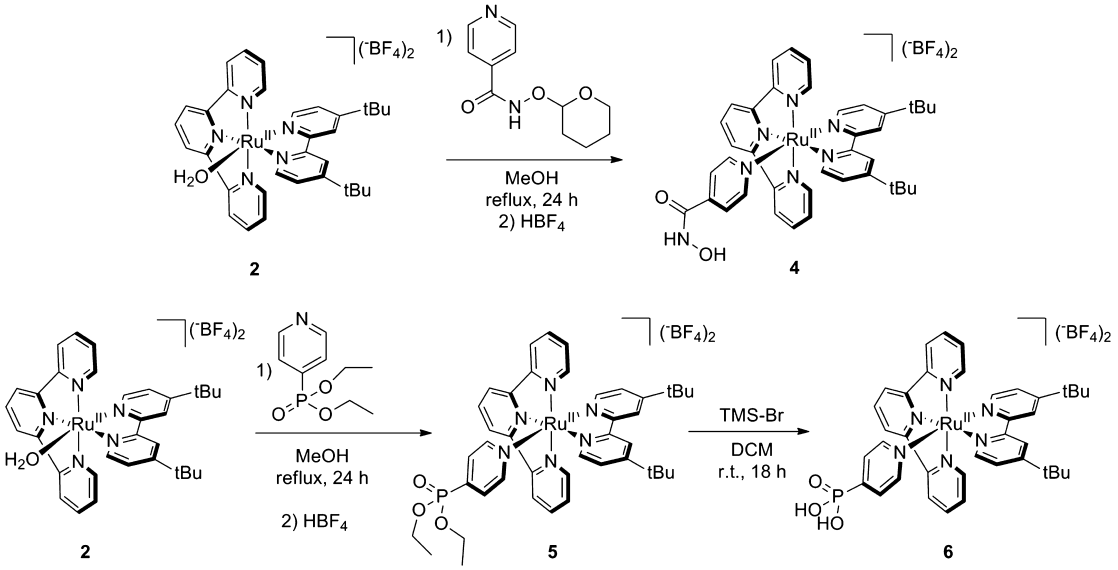

are shown to give the highest overall sunlight-to-electricity conversion efficiency (η), while acetylacetonate dyes are shown to be susceptible to decomposition, limiting their potential in DSSC applications. We propose, based on our findings, that hydroxamate anchors are a viable, synthetically accessible alternative to carboxylates for future artificial photosynthesis devices.

RESULTS AND DISCUSSION

Synthesis and Characterization. Recently we published a report detailing thiocyanate linkage isomerism in [Ru(terpy)(tbbpy)SCN][SbF_6].[42] In the synthesis of this complex, halide was first abstracted from the chloride precursor, [Ru(terpy)(tbbpy)Cl]Cl (**1**), in ethanol and potassium thiocyanate added to the resulting solvento intermediate. Using this route as a model, we were able to isolate the aqua complex [Ru(terpy)(tbbpy)OH_2][BF_4] (**2**) after anion metathesis with silver tetrafluoroborate in a 3:1 mixture of acetone and water. The bound water can then exchange with other ligands, but only slowly at room temperature. Full conversion to the dimethyl sulfoxide complex in d_6-dimethyl sulfoxide requires several hours, as shown by ^{1}H NMR data. As a result of this ligand exchange and the limited solubility of the aqua complex in water, we were unable to record a ^{13}C NMR spectrum of the aqua complex, **2**.

Encouraged by this isolation of **2**, we then set out to synthesize complexes of the form [Ru(terpy)(tbbpy)(pyr-L)][BF_4]$_2$ where pyr-L is isonicotinic acid (pyr-COOH), N-hydroxyisonicotinamide (pyr-hydrox), pyridin-4-ylphosphonic acid (pyr-phos), and 3-(pyridin-4-yl)pentane-2,4-dione (pyr-acac) so as to equip the complex with a series of anchor groups. The complex [Ru(terpy)(tbbpy)(pyr-COOH)][BF_4]$_2$ (**3**) was generated in good yield by adding an excess of isonicotinic acid to **2** in refluxing methanol (Scheme 1). Unfortunately, simple addition of pyr-hydrox or pyr-phos[39] to the starting aqua species generated an inseparable mixture of products.

Assuming that the problem with the hydroxamate and phosphonate syntheses was caused by unwanted coordination of the acid groups to ruthenium, a protection−deprotection strategy was devised. Refluxing tetrahydropyran-protected pyr-hydrox[43] and **2**, in the presence of silver tetrafluoroborate in methanol, followed by washing with aqueous tetrafluoroboric acid, generated [Ru(terpy)(tbbpy)(pyr-hydrox)][BF_4]$_2$ (**4**) in a two-step, one-pot synthesis. The ethyl-protected phosphonate complex, [Ru(terpy)(tbbpy)(pyr-PO(OEt)$_2$)][BF_4]$_2$ (**5**), was likewise generated by addition of pyridin-4-yldiethylphosphonate (pyr-PO(OEt)$_2$)[44] to **2** in refluxing methanol in the presence of silver tetrafluoroborate. Exposure of **5** to bromotrimethylsilane in dry dichloromethane yielded the desired phosphonate complex, [Ru(terpy)(tbbpy)(pyr-phos)][BF_4]$_2$ (**6**) (Scheme 2).

Synthesis of the 3-(pyridin-4-yl)pentane-2,4-dione complex proved to be much more difficult. Pyr-acac was synthesized by a literature method, recrystallized from hexanes, and isolated as a white crystalline solid.[45] However, on standing at room temperature, the solid rapidly decomposed to 1-(4-pyridinyl)-propan-2-one (pyr-acetone), presumably in a water-assisted deacetylation. As a result of this decomposition, addition of pyr-acac to **2** in refluxing methanol always generated a mixture of [Ru(terpy)(tbbpy)(pyr-acac)][BF_4]$_2$ (**7**) and [Ru(terpy)-

dx.doi.org/10.1021/ic4010856 | Inorg. Chem. 2013, 52, 6752−6764

Scheme 3. Attempted Syntheses of [Ru(terpy)(tbbpy)(pyr-acac)][BF_4]$_2$ (7)[46,47]

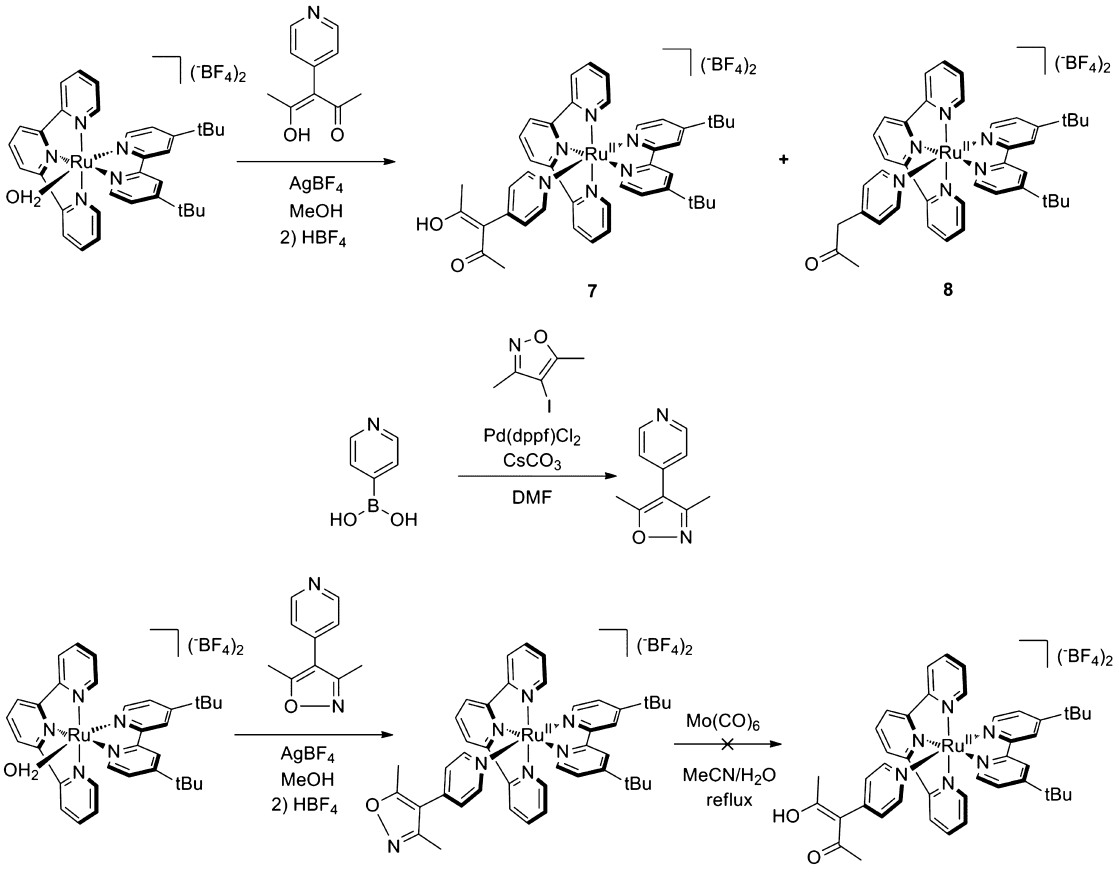

Scheme 4. Synthesis of [Ru(terpy)(tbbpy)(im-ph-COOH)][BF_4]$_2$ (10)

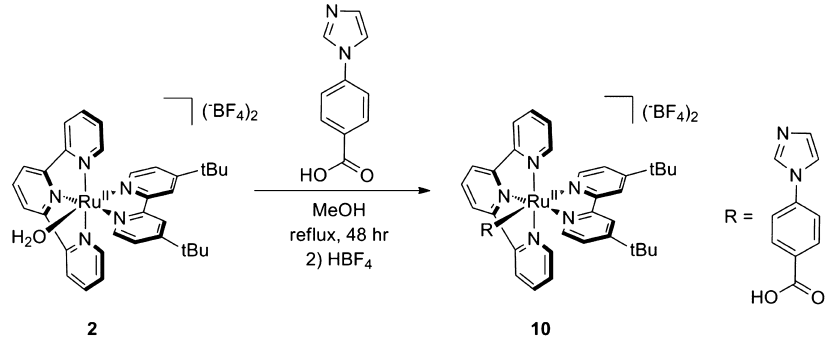

(tbbpy)(pyr-acetone)][BF_4]$_2$ (**8**) consisting mostly of the pyr-acetone complex. Instead, a strategy for synthesizing aryl acetylacetonates from 3,5-dimethylisoxazole precursors was explored.[46] However, the conversion of the ruthenium-bound 3,5-dimethyl-4-(pyridin-4-yl)isoxazole to pyr-acac, which requires vigorous reflux in the presence of $Mo(CO)_6$[47] or other harsh conditions,[46] was unsuccessful (Scheme 3).

Unsure if the mixture of complexes **7** and **8** would lead to a mixture of surface bound complexes as well, we set out to synthesize **8** in pure form. Addition of 1-(pyridin-4-yl)propan-2-one to **2** in refluxing methanol generated **8** in modest yield. Unfortunately, titanium dioxide films sensitized with **8** did show visible absorption indicating a weak interaction with the semiconductor surface (vide infra). To examine if this adsorption was covalent or electrostatic, the complex [Ru(terpy)(tbbpy)-(pyridine)][BF_4]$_2$ (**9**) was synthesized in a similar manner. Even without an anchoring moiety, the pyridine complex (**9**) exhibited a similar visible absorption as **8** on the surface of titanium dioxide indicating that an electrostatic interaction could be sufficient for weak binding (vide infra). This does not, however, exclude the possibility of the tautomerization of **8** to the enol followed by deprotonation in the presence of titanium dioxide to form the enolate, which could subsequently bind the metal oxide surface.

Comparing the performance of all four anchoring groups was complicated by the instability of pyr-acac, and led us to switch from pyridine-based ligands to N-phenylimidazole-based ligands. N-phenylimidazole was chosen for its greater length, possibly allowing for better accessibility of the anchoring moiety to the titanium dioxide surface, and because its lone pairs are slightly more basic than those of pyridine, which could help stabilize coordination of this monodentate ligand to ruthenium during solar cell operation. Synthesis of the carboxylate complex was achieved by refluxing 4-(1*H*-imidazol-1-yl)benzoic acid (im-ph-COOH) and **2** in ethanol for 48 h to form [Ru(terpy)(tbbpy)-

dx.doi.org/10.1021/ic4010856 | *Inorg. Chem.* 2013, 52, 6752−6764

Scheme 5. Synthesis of $[Ru(terpy)(tbbpy)(im\text{-}ph\text{-}hydrox)][BF_4]_2$ (12) and $[Ru(terpy)(tbbpy)(im\text{-}ph\text{-}phos][BF_4]_2$ (15)

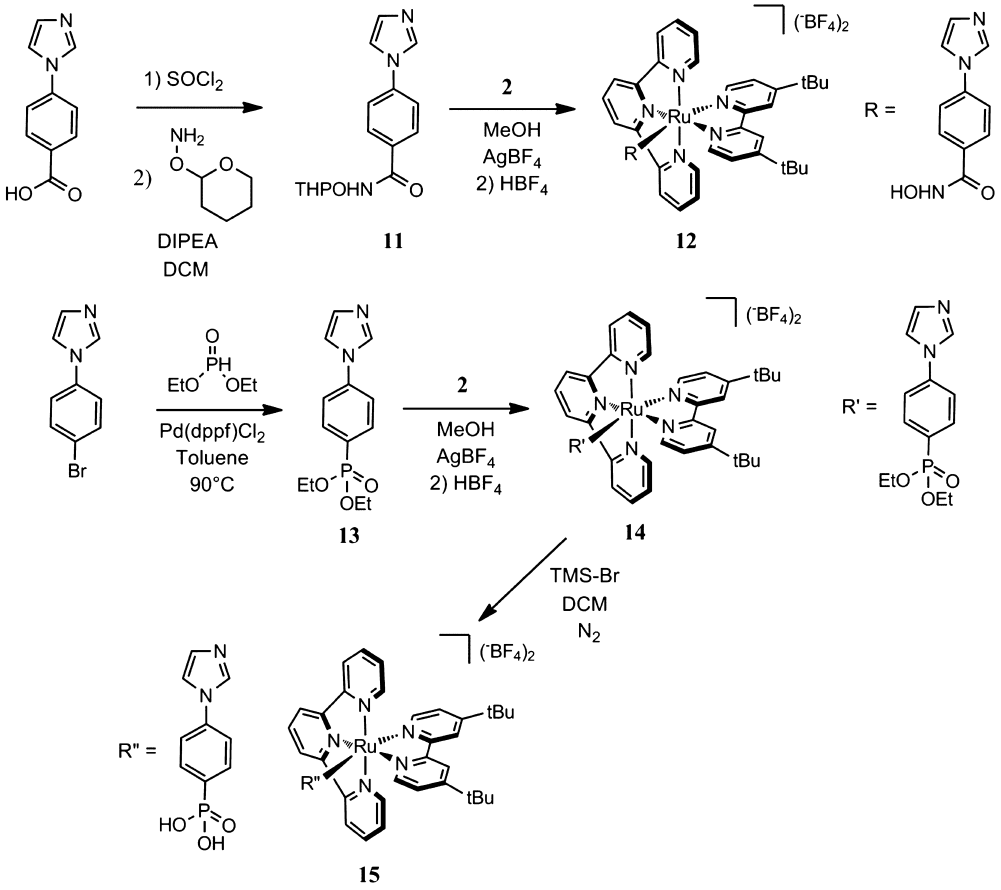

Scheme 6. Attempted Synthesis of $[Ru(terpy)(tbbpy)(im\text{-}ph\text{-}acac)][BF_4]_2$ Yielding a Mixture of 18 and 19

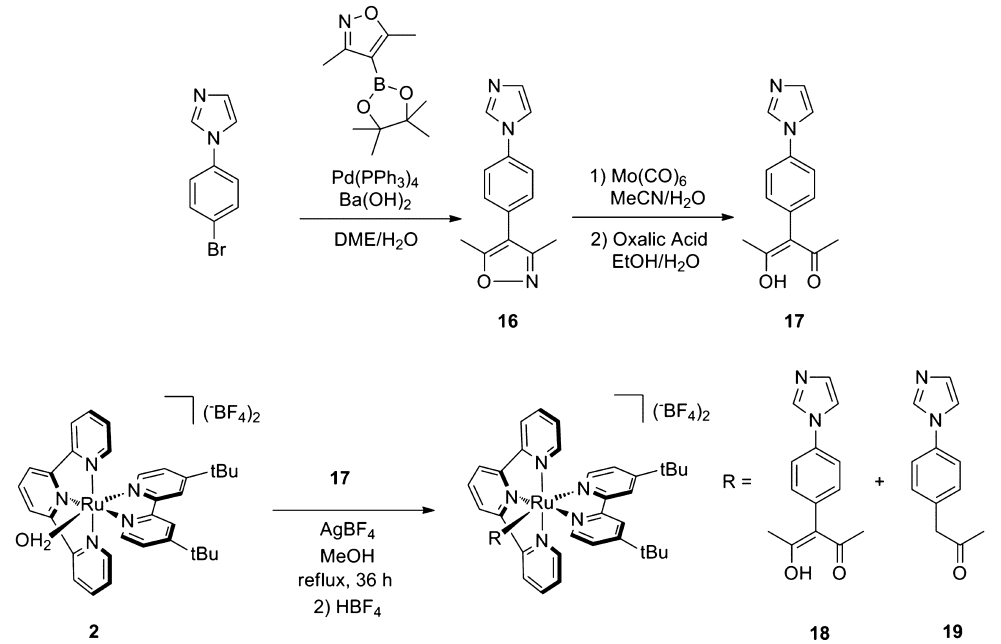

(im-ph-COOH)][BF_4]$_2$ (**10**) (Scheme 4) by a route analogous to the pyr-COOH synthesis.

The hydroxamate and phosphonate N-phenylimidazole complexes were also obtained in a procedure similar to that used for their pyridyl analogues. 4-(1*H*-imidazol-1-yl)-*N*-((tetrahydro-2*H*-pyran-2-yl)oxy)benzamide (**11**) was made from 4-(1*H*-imidazol-1-yl)benzoic acid by conversion to the acid chloride in neat thionyl chloride followed by treatment with O-(tetrahydro-2*H*-pyran-2-yl)hydroxylamine[43] in dry dichloromethane under nitrogen. **11** was then mixed with **2** in refluxing

dx.doi.org/10.1021/ic4010856 | *Inorg. Chem.* 2013, 52, 6752−6764

methanol in the presence of silver tetrafluoroborate. After washing with aqueous HBF_4, [Ru(terpy)(tbbpy)(im-ph-hydrox)][BF_4]$_2$ (im-ph-hydrox = *N*-hydroxy-4-(1*H*-imidazol-1-yl)benzamide) (**12**) was obtained (Scheme 5).

Similarly, diethyl(4-(1*H*-imidazol-1-yl)phenyl)phosphonate (im-ph-(PO(OEt)$_2$, **13**), which was formed by cross-coupling 1-(4-bromophenyl)-1*H*-imidazole and diethyl phosphite in toluene in the presence of triethylamine and Pd(dppf)-Cl_2·dichloromethane (dppf = 1,1′-*bis*-diphenylphosphinoferrocene) as catalyst,[48] was mixed with **2** in refluxing methanol in the presence of silver tetrafluoroborate to give [Ru(terpy)(tbbpy)-(im-ph-PO(OEt)$_2$][BF_4]$_2$ (**14**). Treatment of **14** with bromotrimethylsilane[44] in dichloromethane yielded the deprotected phosphonic acid complex, [Ru(terpy)(tbbpy)(im-ph-phos]-[BF_4]$_2$ (**15**) (im-ph-phos = (4-(1*H*-imidazol-1-yl)phenyl)-phosphonic acid) (Scheme 5).

Finally, a strategy for synthesizing the acetylacetonate N-phenylimidazole complex, again from its 3,5-dimethylisoxazole precursor, was explored. Suzuki coupling of 1-(4-bromophenyl)-1*H*-imidazole and 4-(4,5-dimethyl-1,3,2-dioxaborolan-2-yl)-3,5-dimethylisoxazole using Pd(PPh_3) and Ba(OH)$_2$[47] as base in a 9:1 mixture of dimethoxyethane and water gave 4-(4-(1*H*-imidazol-1-yl)phenyl)-3,5-dimethylisoxazole (**16**). Treatment of **16** with Mo(CO)$_6$ in vigorously refluxing acetonitrile/water (1:1, v:v) followed by addition of oxalic acid in aqueous ethanol yielded 3-(4-(1*H*-imidazol-1-yl)phenyl)-2,4-pentanedione (im-ph-acac, **17**) in high purity after several recrystallizations from hexanes. **17** is a white crystalline solid and, unlike its pyridyl analogue, is stable for several weeks at room temperature or indefinitely if stored in a freezer. All attempts to metalate **17** resulted in a mixture of the desired im-ph-acac product **18** and its deacetylated analogue **19**. Unfortunately, **18** could not be isolated from the mixture (Scheme 6).

Because of these synthetic difficulties and the need for analytically pure material, we then stopped pursuit of the acetylacetonate complexes. This deacetylation pathway is likely to hinder other systems seeking to use acetylacetonate functionalized at the 3 position to anchor sensitizers to titanium dioxide. In the best case, it will limit yields of synthesized dyes, and in the worst case, as we have observed here, it could make synthesis of pure species impossible.

Spectroscopic Characterization. The visible absorption characteristics of our catalog of complexes were measured in two ways. First, absorption spectra were recorded in ethanol solution at a concentration of 0.1 mM. Results are displayed in Figure 2, and show similar spectral characteristics for all of the synthesized complexes, regardless of the anchoring moiety present. Complexes with pyridyl-based anchoring ligands show two absorbance maxima, at 425 and 466 nm, with maximal molar extinction coefficients between 8000 and 10300 M^{-1} cm^{-1}. Complexes with imidazole-based anchoring ligands have red-shifted absorbance maxima, resulting in a broad peak with shoulders at either 469 or 488 nm. Molar absorptivities for the imidazole complexes range between 7200 and 8800 M^{-1} cm^{-1}.

Next, emission spectra and cyclic voltammograms of dyes **3**, **4**, and **6** bearing pyridyl ligands were recorded (see Supporting Information). The aqua complex, **2**, was also investigated in this manner. As can be seen in Figure 3, the energy levels for both the ground state oxidation ($E_{1/2}$) and the first excited state (S^*) are not greatly perturbed by the variation in the anchoring moiety. Interestingly, the spectra of **2** also show very similar ground and excited state energies. Importantly, each of the newly synthesized dyes has an excited state which is poised to inject electrons into

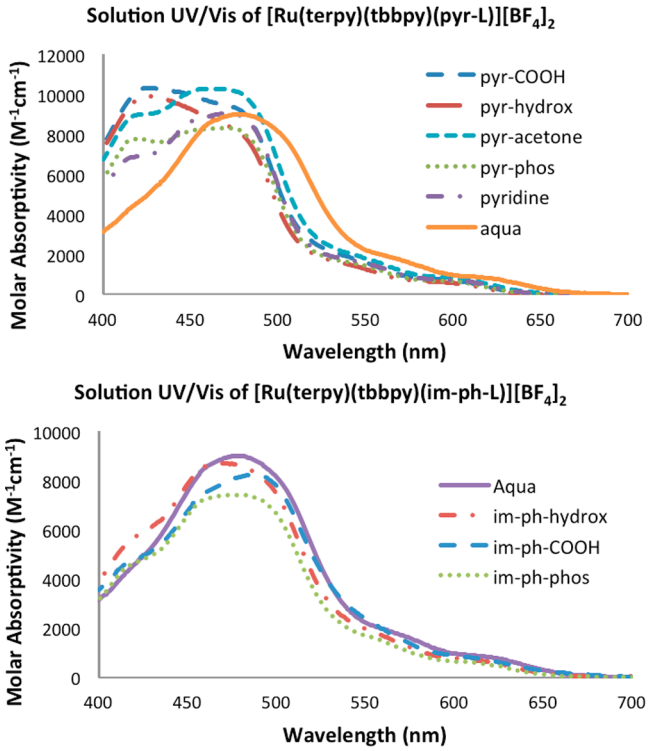

Figure 2. UV/visible spectra of newly synthesized dyes in 0.1 mM ethanol solution. Top: [Ru(terpy)(tbbpy)(pyr-L)]$^{2+}$. Bottom: [Ru-(terpy)(tbbpy)(im-ph-L)]$^{2+}$. [Ru(terpy)(tbbpy)(OH_2)]$^{2+}$ is shown in both graphs as a reference.

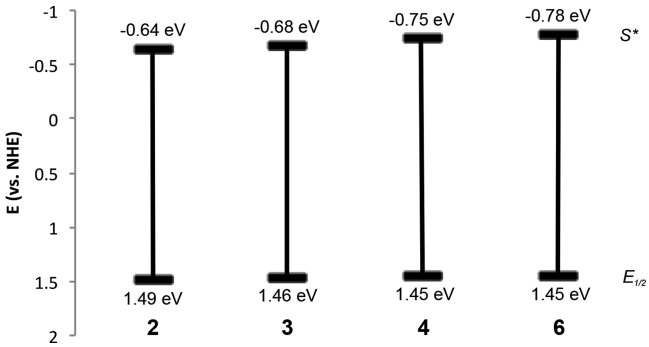

Figure 3. Measured energies of the ground and excited states of **2**, **3**, **4**, and **6**. Ground state energies were measured by cyclic voltammetry as 0.3 mM solutions in acetonitrile. 0.1 M NBu_4BF_4 was used as supporting electrolyte. Fc^+/Fc (0.63 V vs NHE) was used as an internal standard. Emission spectra were recorded as 0.1 mM solutions in ethanol using an excitation wavelength of 475 nm. S^* (S_{0-0}) was measured (or extrapolated) as the intersection point of the lowest energy absorbance and emission features. For full spectra see Supporting Information.

TiO_2 and a ground state which is thermodynamically capable of oxidizing I^- to close the circuit in a functioning DSSC. Given the similarities between these dyes, it can be assumed that dyes **10**, **12**, and **15** will also not show great variance in their electronic characteristics.

Finally, to determine how the absorbance features of the complexes change upon binding to TiO_2, visible absorption spectra of nanoparticle films sensitized with the dye molecules were recorded (Figure 4). For the most consistent and comparable data, films for UV/vis were made by spin-coating colloidal titanium dioxide (1.0 g TiO_2 suspended in 4 mL of 1:1

dx.doi.org/10.1021/ic4010856 | Inorg. Chem. 2013, 52, 6752−6764

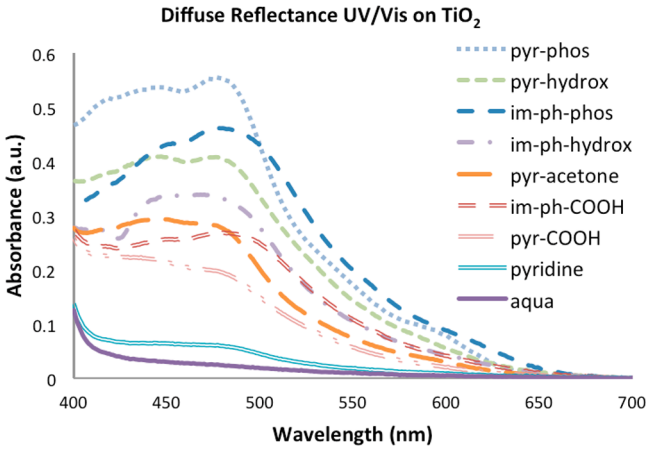

Figure 4. Diffuse reflectance UV/vis of newly synthesized dyes adsorbed onto TiO_2. Slides were soaked in 0.3 mM dye solutions in ethanol for 36 h prior to recording.

ethanol:water) onto glass coverslips at 1000 rpm. Films were then sintered at 450 °C for 2 h. Finally, slides were soaked in 0.3 mM ethanolic solutions of dye for 36 h to ensure maximum coverage. Because the spectra were recorded using diffuse reflectance with an integrating sphere we cannot directly estimate dye surface coverage from the UV−vis data. However, the spectra were highly reproducible for sensitized films prepared from the same dye solution across multiple sample preparations. Thus, it would seem that there is differentiation among the various anchoring moieties in their ability to bind the surface. Our data are consistent with previous work suggesting a higher TiO_2 binding affinity for phosphonates compared to carboxylates.[23,35,49]

The presence of any absorbance features in the visible region indicates the presence of dye on the surface of titanium dioxide. This is especially significant in the cases of aqua complex **2**, pyr-acetone complex **8**, and pyridine complex **9** as they do not bear traditional anchoring groups. We believe that they are most likely held near the surface by electrostatic attraction between the dicationic complex and anionic oxygen atoms on the oxide surface. Such complexes would not be expected to perform as well in photoelectrochemical cells as those bearing anchoring groups that coordinate the metal oxide surface because of a lack of direct electronic communication between the complex and the nanoparticulate surface (vide infra).

In general, the absorption spectra of the ruthenium-polypyridyl dyes bearing varying anchoring groups are not much altered by titanium dioxide sensitization. This is likely because the anchoring group does not play a significant role in the metal-to-ligand charge transfer responsible for the transitions observed in the visible region. Also, the wavelengths of maximum absorption are conserved for both sets of complexes on the semiconductor surface. For dyes bearing pyridyl ligands, the λ_{max} are centered at 476 and 444 nm. For dyes bearing N-phenylimidazole ligands, the absorption maximum appears at 477 nm with a shoulder at 450 nm. This conservation of absorption features among the different photosensitizers is essential to compare their relative performance in dye-sensitized solar cells.

Photovoltaic Cell Current Density−Voltage Characteristics. Solar cells were constructed using the newly synthesized series of ruthenium complexes bearing varying anchoring groups. A 7-μm film of titanium dioxide was deposited on fluorine-doped tin oxide (FTO) conducting glass by spin coating (see Experimental Details). The mesoporous TiO_2 film was reduced in area to approximately 0.5 cm by 0.5 cm by removing excess titanium dioxide using a template, then scanned to calculate surface area with higher accuracy. The electrodes were then soaked in 0.3 mM solutions of dye for a minimum of 3 days to ensure maximum surface coverage. A platinized counter-electrode was fashioned by a previously described method.[41] Cells were then assembled using our electrodes separated by a 60-μm plastic thermal spacer (SX1170-60, Solaronix SA, Switzerland) held together with binder clips. The electrolyte consisted of 0.6 M *tert*-butylammonium iodide, 0.05 M iodine, 0.1 M lithium iodide, and 0.5 M *tert*-butyl pyridine (tBP) in a 1:1 mixture of valeronitrile and acetonitrile. The *J-V* curves were measured in quadruplicate from independent preparations of dye molecule and sensitization.

Representative *J-V* curves for solar cells sensitized with each new dye are shown in Figure 5, and all photovoltaic parameters are reported in Table 1. We also report the *J-V* curve and corresponding parameters for a TiO_2 anode sensitized with N719[13] operating under our conditions.

Table 1 shows that the hydroxamate anchors give the best overall efficiencies for both the pyridyl- and the N-phenyl-

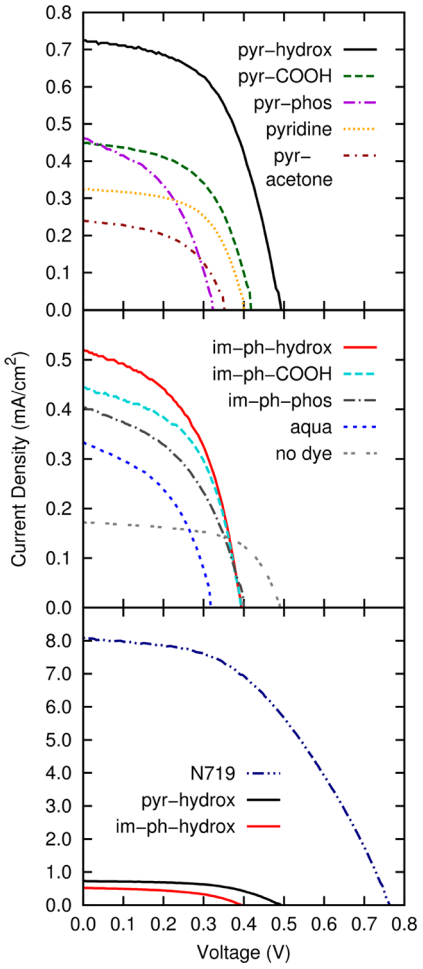

Figure 5. Experimental current density−voltage curves of representative solar cells based on the newly synthesized $[Ru(terpy)(tbbpy)(R)]^{2+}$ dye molecules. Top: R = pyr-L or pyridine; Middle: Cell containing bare TiO_2 or dyes where R = im-ph-L or aqua; Bottom: Comparison of hydroxamate-anchored dyes with N719.

dx.doi.org/10.1021/ic4010856 | *Inorg. Chem.* 2013, 52, 6752−6764

Table 1. Measured Characteristics and Calculated Fitting Parameters of Solar Cells Based on the New Dyes[a]

dye	R	J_{sc} (mA/cm^2)	V_{oc} (V)	*FF*	η (%)	J_L (mA/cm^2)	J_0 (mA/cm^2)	AR_s (kΩ·cm^2)	AR_{sh} (kΩ·cm^2)
2	aqua	0.29	0.33	0.47	0.05	0.30	3.4×10^{-4}	0.11	4.10
3	pyr-COOH	0.40	0.41	0.54	0.09	0.40	1.2×10^{-4}	0.10	7.39
4	pyr-hydrox	0.70	0.51	0.55	0.20	0.72	3.7×10^{-5}	0.096	5.94
6	pyr-phos	0.43	0.32	0.43	0.06	0.44	6.3×10^{-4}	0.073	2.28
8	pyr-acetone	0.23	0.34	0.51	0.04	0.24	2.2×10^{-4}	0.094	7.50
9	pyridine	0.31	0.40	0.57	0.07	0.32	1.1×10^{-4}	0.069	12.10
10	im-ph-COOH	0.41	0.39	0.51	0.08	0.42	1.7×10^{-4}	0.082	4.46
12	im-ph-hydrox	0.51	0.38	0.48	0.09	0.53	2.2×10^{-4}	0.072	2.75
15	im-ph-phos	0.39	0.38	0.45	0.07	0.41	1.9×10^{-4}	0.15	3.18
blank		0.16	0.47	0.60	0.05	0.16	1.6×10^{-5}	0.029	20.44
N719		7.52	0.73	0.54	2.91	7.76	6.0×10^{-6}	0.025	1.14

[a]Reported values are the average of values obtained from two to four cells across multiple preparations.

imidazole-based complexes. Consistent with their poor electron injection,[34,35] the phosphonate complexes showed the lowest overall solar-to-electric conversion. Meanwhile, the carboxylate-anchored complexes showed intermediate conversion. It is notable that all of our measured efficiencies for the newly synthesized dyes are an order of magnitude lower than those measured for N719. However, the low efficiency of our dye molecules only serves to magnify the relative effect of the anchoring moiety. It is likely that the observed increases in efficiency would be conserved in "champion" solar dyes upon switching from carboxylate to hydroxamate, though the relative percent increase in efficiency would be lower. Investigations of highly efficient dyes with hydroxamate anchors are currently underway.

Further insight into the anchor-dependent TiO_2 surface chemistry, device photophysics, and cell electrochemistry can be gained by analyzing the solar cell *J-V* characteristics with an equivalent circuit model. Parameters readily obtained from the experimental data such as the short-circuit photocurrent, open-circuit voltage, and fill factor of the cell provide a useful starting point for comparison as they ultimately make up the solar-to-electrical energy conversion efficiency. However, direct relation of these parameters to the many device processes that influence them is difficult. The equivalent circuit model breaks down the complexity of the DSSC into components, thus unraveling the various fundamental processes controlling device efficiency and enabling them to be studied and compared independently.

The device parameters shown in Table 1 were extracted from the *J-V* curves based on the equivalent circuit shown in Figure 6 and the modified nonideal diode equation:[41,50]

$$J = J_L - J_0\left\{\exp\left[\frac{e(V + JAR_s)}{nkT}\right] - 1\right\} - \frac{V + JAR_s}{AR_{sh}} \qquad (2)$$

where J_L is the photogenerated current density, R_s is the series resistance, kT is the thermal energy, e is the elementary charge, A is the device area, and n is the ideality factor. The solar cell shunt resistance R_{sh} and reverse saturation currents J_0 are parameters extracted from the *J-V* curves that quantify the various loss mechanisms in solar cells. High leakage currents in DSSCs are generally attributed to undesired recombination of carriers with the redox mediator in the electrolyte, either at regions of FTO directly exposed to the electrolyte or, the putative more dominant mechanism, via the nanoporous metal oxide. Increasing the device shunt resistance improves device efficiency because of both higher fill factors and larger open circuit voltages. A global value of the ideality factor ($n = 2$) was used in this

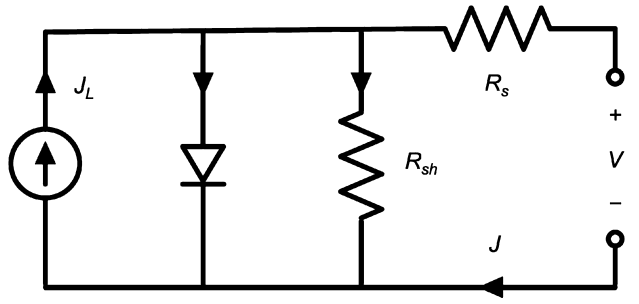

Figure 6. Equivalent circuit for modeling solar cells using the modified nonideal diode equation [eq 1]. The net current density J depends on the net series resistance R_s of the cell and is composed of the photogenerated current density J_L (defined in the forward direction) and two back-flowing current densities competing with J_L: a diode current density with exponential voltage dependence and a shunt current density with ohmic resistance R_{sh}.

systematic study for better comparison of J_0 values. Table 1 shows that the values of the series resistance, which result primarily from the electrode and ionic resistances of the cell, are similar for all devices, indicating that the fabrication procedure yields consistent metal oxide film thickness and porosity (as confirmed experimentally[39]). Equation 1 has been used to model *J-V* characteristics in a wide variety of solar cell technologies including hydrogenated amorphous silicon p-i-n cells, Cu-(In,Ga)Se_2 cells, organic bulk heterojunction cells, and DSSCs.[41,50−52] This model has been shown to work well for DSSCs, particularly when performing a comparative analysis of a series of device architectures in which cell components are systematically varied,[41] as in the present study.

The biggest systematic difference between the anchoring groups is evident in the J_L values. It is readily apparent from eq 2 that J_L is approximately equal to the photocurrent at zero bias (J_{sc}) for moderate to large shunt resistances. Table 1 shows that the shunt resistance is high enough in all devices as to not greatly affect the short-circuit current ($J_{sc} \approx J_L$). In both the pyridyl and the *n*-phenylimidazole cases, dyes bearing hydroxamate anchors have the highest values of J_L (0.70 and 0.51 respectively), while the carboxylate and phosphonate have very similar, lower calculated values (pyr-COOH = 0.40, pyr-phos = 0.43, im-ph-COOH = 0.41, im-ph-phos = 0.39). Though other factors may also be involved, this suggests that the improved electron injection observed for hydroxamates[25,39] indeed has a measurable effect on the solar cell performance. However, to achieve high overall efficiency, higher J_{sc} and J_L values need to be coupled with low reverse saturation currents and/or high shunt resistance

dx.doi.org/10.1021/ic4010856 | Inorg. Chem. 2013, 52, 6752−6764

to facilitate sustained photocurrent as a function of voltage, that is, larger fill factors and open circuit voltages. Unfortunately, attempts to directly measure electron injection across our series of dye molecules by THz spectroscopy suffered from a poor signal-to-noise ratio resulting from the low amount of carriers generated by dye excitation.

Looking at the performance of the newly synthesized dyes as a whole, solar cells based on the pyridyl-hydroxamate anchor not only give the highest photoinjection current densities but they are also significantly more efficient. The average measured efficiency is 0.20%, while all other dyes, including the N-phenylimidazole-hydroxamate-based complex, give efficiencies in the range of 0.04−0.09%. Given this great difference, it is not surprising that the pyr-hydrox cell also has a reverse saturation current that is significantly lower than all the rest. This indicates that, in addition to the photophysical properties of the attached dye, the hydroxamate anchor increases suppression of electron transfer from the photoanode to the electrolyte.

The trends in R_{sh} and J_0 in Table 1 are also consistent with expected surface binding and its mitigation of the effects of tBP. The addition of 0.5 M tBP to the DSSC electrolyte solution, as is common practice in the literature, is known to increase the V_{oc},[6,14,53−56] and is attributed, in part, to a decrease in the amount of electron recombination in TiO_2 by blocking access of triiodide to the TiO_2 surface and/or by iodine complexation.[54] These effects can account for an increase in the R_{sh}, which is evident from the *J-V* curves showing a decrease in the magnitude of the slope of the current density at low voltages. A second effect of tBP is a lowering of the reverse saturation current density J_0, as observed by a shift in the sharp onset of the recombination current (near $V = V_{oc}$) to higher voltages.[6,56] This can be explained by a decrease in the number of positive ions (protons and Li^+) adsorbed to the TiO_2 surface, leading to a shift in the conduction band minimum of nanoporous TiO_2 to higher energies (more negative potentials).[14,53−55] The hydroxamate-, carboxylate-, and phosphonate-anchored complexes in the present study have lower shunt resistances compared to cells made with unsensitized TiO_2 photoanodes, which is consistent with dye attachment interfering with the ability of tBP to block recombination sites on the TiO_2 surface. The values of J_0 are generally larger since binding of dye molecules competes with tBP and its effect on the conduction band minimum of TiO_2. The pyr-hydrox anchor seems to be the exception since it has a larger photoinjection current density, while maintaining a low J_0.

It is also interesting to note that solar cells sensitized with the pyridine complex **9** give an appreciably larger photoresponse than unsensitized cells. This suggests that an electrostatic attraction with the semiconductor surface is not only sufficient for binding dye molecules, but that it also can hold sensitizers tightly enough to facilitate through-space electron transfer. It is notable that pyr-acetone complex **8** gives a lower overall sunlight-to-electricity conversion efficiency than **9** with a very similar value calculated for J_0. This suggests that the association of **8** to the semiconductor surface may not be covalent. However, a tautomerization to the enolate form of pyr-acetone followed by weak binding through an alkoxide cannot be excluded. Unfortunately, this also prohibits titanium dioxide sensitization using a mixture of **7** and **8** or **18** and **19**. While it is likely that binding acetylacetonate to titanium dioxide would be thermodynamically preferred over either the alkoxide or a pure electrostatic attraction, it is impossible to rigorously prove that all surface-bound molecules resulting from a sensitizing mixture bear acetylacetonate moieties. Additionally, because some current could be derived from deacetylated species adsorbed to TiO_2, we cannot say that *all* photocurrent was obtained from the desired acetylacetonate complexes. This reinforces the need for analytically pure dyes in sensitization,[57] and severely diminishes the utility of acetylacetonate as an anchor for DSSC applications. Unless an analogue is found in which the acetylacetonate does not deacetylate under solution conditions, or where it can be proven that the deacetylated species has no interaction with the semiconductor surface, acetylacetonate should not be used.

In regard to solar fuels production, it is highly advantageous that the hydroxamate species produce the best measured efficiencies (η). Hydroxamate anchors, unlike carboxylates, are stable under aqueous conditions over a wide range of pH values when the corresponding dye is soluble in water.[25,39] This feature will be essential for any water-oxidation/proton reduction dye-sensitized solar cell.[15] It would seem that, owing to the relative ease of synthesis, strong binding, compatibility with water oxidation catalysis, and the relatively high overall photovoltaic efficiency afforded, a hydroxamate anchor is a leading candidate for any dye molecule to be used in a photoelectrochemical water oxidation cell.

■ CONCLUSIONS

Our analysis of a series of anchoring groups for covalent attachment of ruthenium-polypyridyl dyes of the form $[Ru(terpy)(tbbpy)L][BF_4]_2$ to TiO_2 surfaces predicts that hydroxamate anchors should lead to improved performance of DSSCs. Solar cells were constructed by using newly synthesized photosensitizers and tested under AM 1.5 illumination. Hydroxamic acid anchoring groups were found to give superior photogenerated current densities, when compared to other anchors, including carboxylate groups used in traditional DSSCs. Analysis by the nonideal diode equivalent circuit model shows that solar cells based on the pyridyl-hydroxamate anchor give significantly higher efficiencies because the current density−voltage characteristics show increased suppression of electron transfer from the photoanode to the electrolyte. In addition, we see better photoinjection properties that are characteristic of the hydroxamate anchor. Since hydroxamates provide stable attachment in aqueous environments and have demonstrated improved performance over carboxylates in this system, they are a good candidate for applications in artificial photosynthesis devices.

■ EXPERIMENTAL DETAILS

$Ru(terpy)Cl_3$,[58] $[Ru(terpy)(tbbpy)(Cl)]Cl{\cdot}H_2O$ (**1**),[42] and diethyl pyridin-4-ylphosphonate[39] were synthesized by literature methods. Dichloromethane, toluene, and acetonitrile were dried on a Grubbs-type solvent purification system.[59] All other reagents and solvents were commercially available and used without further purification unless specified. Deuterated solvents were purchased from Cambridge Isotope Laboratories and used as received. ^1H NMR spectra were recorded on a 400 MHz Bruker spectrometer and referenced to the residual solvent peak (δ in ppm, *J* in Hz). $^{13}C\{^1H\}$ NMR spectra were recorded on a 500 MHz Varian or Bruker spectrometer and referenced to the solvent peak. ^{31}P NMR spectra were recorded on a 300 MHz Varian spectrometer. High-resolution ESI mass spectra were collected by the Mass Spectrometry and Proteomics Resource at the W.M. Keck Foundation Biotechnology Resource Laboratory (Yale University). Elemental analysis was performed by Robertson Microlit Laboratories (Ledgewood, NJ) and Atlantic Microlab, Inc. (Norcross, GA).

$[Ru(terpy)(tbbpy)(OH_2)][BF_4]_2$ (2). A 2.018 g portion (2.99 mmol) of $[Ru(terpy)(tbbpy)Cl]Cl$ and 1.947 g (10.0 mmol) of silver tetrafluoroborate were dissolved in 200 mL of 3:1 acetone:water. The

dx.doi.org/10.1021/ic4010856 | Inorg. Chem. 2013, 52, 6752−6764

resulting solution was refluxed overnight in the dark under air. The volume of the solution was then reduced to approximately 25 mL, and 5 mL of 48 wt % HBF_4 (aq.) was added. The resulting suspension was cooled in a freezer for 1 h. The brown precipitate was then filtered off, washed with 1 M HBF_4 (aq.), and dried. The dimethyl sulfoxide adduct was prepared by dissolving $[Ru(terpy)(tbbpy)(OH_2)][BF_4]_2$ in d_6-dimethyl sulfoxide and letting the solution stand for 3 h. Yield: 1.593 g, 67%. ^{1}H NMR (400 MHz, DMSO) δ 9.38 (d, J = 6.0 Hz, 1H), 8.99 (d, J = 1.7 Hz, 1H), 8.87 (d, J = 8.1 Hz, 2H), 8.73 (d, J = 8.0 Hz, 2H), 8.68 (d, J = 1.9 Hz, 1H), 8.31 (t, J = 8.1 Hz, 1H), 8.15 (dd, J = 6.0, 1.9 Hz, 1H), 8.06 (td, J = 7.9, 1.4 Hz, 2H), 7.69−7.64 (m, 2H), 7.49−7.42 (m, 2H), 7.13 (d, J = 6.1 Hz, 1H), 7.06 (dd, J = 6.2, 2.1 Hz, 1H), 5.80 (s, 2H), 1.61 (s, 9H), 1.22 (s, 9H). ^{1}H NMR (501 MHz, DMSO, DMSO adduct) δ 9.87 (d, J = 6.1 Hz, 1H), 8.97−8.90 (m, 3H), 8.78−8.73 (m, 3H), 8.57 (t, J = 8.1 Hz, 1H), 8.18 (t, J = 7.7 Hz, 2H), 8.09 (dd, J = 6.0, 1.5 Hz, 1H), 7.80 (d, J = 5.3 Hz, 2H), 7.53 (t, J = 6.5 Hz, 2H), 7.34−7.29 (m, 1H), 6.96 (d, J = 6.1 Hz, 1H), 1.56 (s, 9H), 1.25 (s, 9H). ^{13}C{^{1}H} NMR (126 MHz, DMSO, DMSO adduct) δ 163.18, 162.48, 157.18, 156.76, 155.44, 155.13, 154.12, 153.46, 148.02, 139.31, 138.45, 128.83, 125.53, 125.10, 124.71, 124.36, 122.00, 121.40, 35.60, 35.42, 30.19, 29.76. Elemental Analysis for $C_{33}H_{37}B_2F_8N_5ORu$: Calculated: C 49.90; H 4.69; N 8.82. Measured: C 49.76; H 4.43; N 8.73.

[Ru(terpy)(tbbpy)(pyr-COOH)][BF$_4$]$_2$ (3). A 98 mg portion (0.123 mmol) of $[Ru(terpy)(tbbpy)(OH_2)][BF_4]_2$ (**2**) and 82 mg (0.723 mmol) of isonicotinic acid were refluxed overnight in 20 mL of methanol. The resulting solution was dried in vacuo. The residual red-brown solid was suspended in 25 mL of 1 M HBF_4 (aq.), collected by filtration, and washed with additional 1 M HBF_4. Yield: 90 mg, 81%. ^{1}H NMR (400 MHz, DMSO) δ 9.01 (d, J = 1.8 Hz, 1H), 8.88 (d, J = 8.2 Hz, 2H), 8.77 (d, J = 7.3 Hz, 3H), 8.55 (d, J = 6.0 Hz, 1H), 8.35 (t, J = 8.1 Hz, 1H), 8.14 (td, J = 7.9, 1.4 Hz, 2H), 7.98−7.95 (m, 1H), 7.82 (d, J = 4.8 Hz, 4H), 7.60−7.52 (m, 4H), 7.17 (d, J = 0.9 Hz, 2H), 1.56 (s, 9H), 1.25 (s, 9H). ^{13}C{^{1}H} NMR (126 MHz, DMSO) δ 164.95, 161.56, 161.40, 157.66, 157.04, 156.60, 155.35, 152.63, 152.40, 150.91, 150.24, 138.58, 136.03, 128.86, 125.11, 124.97, 124.60, 124.04, 123.73, 122.00, 121.29, 35.58, 35.25, 30.26, 29.86. Elemental Analysis for $C_{39}H_{40}B_2F_8N_6O_2Ru$: Calculated: C 52.08; H 4.48; N 9.34. Measured: C 52.35; H 4.32; N 9.26.

***N*-((Tetrahydro-2*H*-pyran-2-yl)oxy)isonicotinamide.** A 495 mg portion (4.02 mmol) of isonicotinic acid was placed under nitrogen in a flame-dried round-bottom flask fitted with a reflux condenser. 11 mL (vast excess) of thionyl chloride was added via syringe. The resulting solution was refluxed for 2 h under nitrogen. Excess thionyl chloride was blown off under a stream of nitrogen through an aqueous potassium carbonate bubbler. The resulting white solid was then dried in vacuo for 30 min. Once dry, the solid was placed back under nitrogen and dissolved in 10 mL of dry dichloromethane. Diisopropylethylamine (1.0 mL) was added. Separately, in a pear-shaped flask under nitrogen, 630 mg of (5.38 mmol) *O*-(tetrahydro-2*H*-pyran-2-yl)hydroxylamine was dissolved in 10 mL of dry dichloromethane. One milliliter of diisopropylethylamine was added to the hydroxylamine precursor, and the resulting solution was added via cannula to the reaction vessel. The reaction was stirred at room temperature for 18 h. After completion, the volatiles were removed yielding an off-white solid. The product was purified chromatographically on silica using 4% methanol in dichloromethane as eluent. Yield: 689 mg, 77%. ^{1}H NMR (501 MHz, CD_2Cl_2) δ 8.68 (d, J = 4.9 Hz, 2H), 7.59 (d, J = 4.5 Hz, 2H), 5.06 (s, 1H), 3.97 (t, J = 9.9 Hz, 1H), 3.67−3.54 (m, 1H), 1.88−1.72 (m, 3H), 1.68−1.53 (m, 4H). ^{13}C{^{1}H} NMR (126 MHz, CD_2Cl_2) δ 163.65, 150.48, 139.55, 121.11, 102.84, 62.72, 28.12, 25.04, 18.68. HRMS for $C_{11}H_{14}N_2O_3^+$ Calculated: 223.10772; Measured: 223.10700.

[Ru(terpy)(tbbpy)(pyr-hydrox)][BF$_4$]$_2$ (4). A 111 mg portion (0.500 mmol) of *N*-((tetrahydro-2*H*-pyran-2-yl)oxy)isonicotinamide and 126 mg (0.649 mmol) of silver tetrafluoroborate were stirred in 20 mL of methanol in the dark for 1 h. A 101 mg portion (0.127 mmol) of $[Ru(terpy)(tbbpy)(OH_2)][BF_4]_2$ (**2**) was added, and the resulting suspension refluxed for 18 h. The resulting suspension was filtered through Celite to remove any precipitate, and the filtrate was dried in vacuo. The resulting red-orange solid was suspended in excess 0.1 M aqueous HBF_4, collected by filtration, and washed with additional 0.1 M aqueous HBF_4. Yield: 68 mg, 59%. ^{1}H NMR (400 MHz, DMSO) δ 9.01 (t, J = 1.7 Hz, 1H), 8.88 (dd, J = 8.1, 2.2 Hz, 2H), 8.79−8.74 (m, 3H), 8.59−8.54 (m, 1H), 8.36 (td, J = 8.1, 3.1 Hz, 1H), 8.20−8.12 (m, 2H), 8.00−7.88 (m, 3H), 7.83 (t, J = 6.2 Hz, 2H), 7.66 (t, J = 6.7 Hz, 1H), 7.60−7.50 (m, 3H), 7.17 (dd, J = 2.7, 1.4 Hz, 2H), 3.81 (s, 1H), 1.56 (s, 9H), 1.25 (s, 9H). ^{13}C{^{1}H} NMR (126 MHz, DMSO) δ 164.87, 163.96, 161.65, 157.65, 157.03, 156.59, 155.39, 153.31, 153.14, 152.70, 152.58, 150.23, 138.69, 137.47, 128.90, 125.04, 124.81, 124.51, 124.09, 123.76, 122.00, 121.32, 35.59, 35.27, 30.26, 29.85. HRMS for $(C_{39}H_{41}N_7O_2Ru)^{2+}$: Calculated: 370.11433; Measured: 370.11923.

[Ru(terpy)(tbbpy)(pyr-PO(OEt)$_2$)][BF$_4$]$_2$ (5). A 100 mg portion (0.126 mmol) of $[Ru(terpy)(tbbpy)(OH_2)][BF_4]_2$ (**2**), 154 mg (0.716 mmol) of diethyl pyridin-4-ylphosphonate, and 194 mg (1 mmol) of silver tetrafluoroborate were refluxed in methanol for 18 h in the dark. The solution was then filtered through Celite, and solvent removed in vacuo leaving a brown solid. The brown solid was suspended in 25 mL of 1 M HBF_4 (aq.), collected by filtration, and washed with additional 1 M HBF_4. Yield: 104 mg, 83%. ^{1}H NMR (400 MHz, DMSO) δ 9.00 (d, 1H), 8.89 (d, J = 8.1 Hz, 2H), 8.77 (d, J = 7.2 Hz, 3H), 8.58 (d, J = 5.9 Hz, 1H), 8.37 (t, J = 8.1 Hz, 1H), 8.15 (t, J = 7.4 Hz, 2H), 7.99−7.93 (m, 3H), 7.82 (d, J = 5.1 Hz, 2H), 7.58−7.45 (m, 4H), 7.17 (m, 2H), 4.06−3.97 (m, 4H), 1.57 (s, 9H), 1.25 (s, 9H), 1.19 (t, J = 7.0 Hz, 6H). ^{13}C{^{1}H} NMR (126 MHz, DMSO) δ 161.71, 161.55, 157.67, 157.05, 156.59, 155.37, 152.73 (d, J = 12.4 Hz), 152.70, 150.98, 150.16, 138.68, 138.30 (d, J = 186.4 Hz), 136.28, 128.91, 127.03 (d, J = 9.2 Hz), 125.04, 124.67, 124.14, 123.81, 121.98, 121.29, 62.86 (d, J = 5.9 Hz), 35.59, 35.25, 30.25, 29.85, 16.06 (d, J = 6.0 Hz). ^{31}P{^{1}H} NMR (202 MHz, DMSO) δ 12.21. HRMS for $(C_{42}H_{49}N_6O_3PRu)^{2+}$: Calculated: 409.1324; Measured: 409.1314.

[Ru(terpy)(tbbpy)(pyr-phos)][BF$_4$]$_2$ (6). A 58 mg portion (0.0585 mmol) of $[Ru(terpy)(tbbpy)(pyr\text{-}PO(OEt)_2)][BF_4]_2$ (**5**) was dissolved in 20 mL of dry dichloromethane under nitrogen. An excess of bromotrimethylsilane (0.3 mL) was then added via syringe, and the solution was stirred at room temperature overnight. Solvent was removed, and the resulting mixture was suspended in 1 M HBF_4 (aq.). A dark brown solid was then collected by filtration, washed with additional HBF_4, and vacuum-dried. Yield: 33 mg, 60%. ^{1}H NMR (500 MHz, DMSO) δ 9.01 (d, J = 1.6 Hz, 1H), 8.87 (d, J = 8.2 Hz, 2H), 8.76 (d, J = 8.8 Hz, 3H), 8.58 (d, J = 6.0 Hz, 1H), 8.34 (t, J = 8.1 Hz, 1H), 8.13 (t, J = 7.9 Hz, 2H), 8.02 (dd, J = 6.0, 1.8 Hz, 1H), 7.82 (d, J = 5.6 Hz, 4H), 7.56−7.51 (m, 2H), 7.39 (dd, J = 11.9, 6.2 Hz, 2H), 7.17 (s, 2H), 1.56 (s, 9H), 1.25 (s, 9H) ^{13}C{^{1}H} NMR (126 MHz, DMSO) δ 161.56, 161.38, 157.62, 157.02, 156.62, 155.36, 152.65, 151.73 (d, J = 12.9 Hz), 150.84, 150.25, 138.55, 137.68 (d, J = 191.4 Hz), 136.01, 128.87, 126.75 (d, J = 8.3 Hz) 125.03, 124.68, 124.11, 123.74, 122.01, 121.30, 35.61, 35.26, 30.29, 29.87. ^{31}P{^{1}H} NMR (122 MHz, DMSO) δ 6.91. HRMS for $(C_{38}H_{41}N_6O_3PRu)^{2+}$: Calculated: 381.10103; Measured: 381.10040.

[Ru(terpy)(tbbpy)(pyr-acetone)][BF$_4$]$_2$ (8). A 50 mg portion (0.063 mmol) of $[Ru(terpy)(tbbpy)(OH_2)][BF_4]_2$ (**2**) and 56 mg (0.423 mmol) of 1-(pyridin-4-yl)propan-2-one were refluxed in 20 mL of methanol for 36 h in the absence of light. Solvent was removed almost to dryness, and a brown solid was precipitated using 48 wt % HBF_4 (aq.). The solid was collected by filtration and washed with 1 M HBF_4 (aq.). Yield: 28 mg, 49%. ^{1}H NMR (400 MHz, DMSO) δ 9.00 (s, 1H), 8.87 (d, J = 8.2 Hz, 2H), 8.79−8.73 (m, 3H), 8.53 (d, J = 6.2 Hz, 1H), 8.34 (t, J = 8.2 Hz, 1H), 8.13 (t, J = 7.7 Hz, 2H), 8.00 (m, 1H), 7.83 (d, J = 5.5 Hz, 2H), 7.66 (d, J = 6.6 Hz, 2H), 7.56−7.49 (m, 2H), 7.18−7.13 (m, 2H), 7.10 (d, J = 6.6 Hz, 2H), 3.85 (s, 2H), 2.13 (s, 3H), 1.56 (s, 9H), 1.25 (s, 9H). ^{13}C{^{1}H} NMR (126 MHz, DMSO) δ 204.37, 162.30, 162.02, 161.76, 158.10, 157.56, 157.13, 155.85, 153.10, 151.49, 150.71, 146.91, 146.04, 144.26, 138.95, 136.30, 129.30, 128.27, 125.43, 124.48, 122.43, 121.73, 104.69, 48.07, 36.08, 35.71, 30.75, 30.32. HRMS for $(C_{41}H_{44}N_6ORu)^{2+}$: Calculated: 369.13101; Measured: 369.13003.

[Ru(terpy)(tbbpy)(pyr)][BF$_4$]$_2$ (9). A 105 mg portion (0.132 mmol) of $[Ru(terpy)(tbbpy)(OH_2)][BF_4]_2$ (**2**) and 115 mg (1.32 mmol) of pyridine were dissolved in 20 mL of methanol and refluxed 18 h. Solvent was removed almost to dryness, and a brown solid was precipitated using 48 wt % HBF_4 (aq.). The solid was collected by filtration and washed with 1 M HBF_4 (aq.). Yield: 44 mg, 39%. ^{1}H NMR (400 MHz, DMSO) δ 9.01 (d, J = 1.9 Hz, 1H), 8.88 (d, J = 8.2 Hz, 2H), 8.79−8.74 (m, 3H), 8.52 (d, J = 6.1 Hz, 1H), 8. 34 (t, J = 8.1 Hz, 1H),

dx.doi.org/10.1021/ic4010856 | *Inorg. Chem.* 2013, 52, 6752−6764

8.14 (td, J = 7.9, 1.5 Hz, 2H), 7.98 (dd, J = 6.0, 2.0 Hz, 1H), 7.89−7.81 (m, 3H), 7.75−7.71 (m, 2H), 7.57−7.51 (m, 2H), 7.34−7.29 (m, 2H), 7.17 (d, J = 1.1 Hz, 2H), 1.56 (s, 9H), 1.25 (s, 9H). $^{13}C\{^1H\}$ NMR (126 MHz, DMSO) δ 161.56, 161.34, 157.67, 157.09, 156.66, 155.39, 152.64, 151.71, 150.75, 150.29, 138.53, 138.18, 135.90, 128.88, 126.47, 124.95, 124.61, 124.00, 123.71, 121.98, 121.28, 35.60, 35.25, 30.27, 29.86. Elemental Analysis for $C_{38}H_{40}B_2F_8N_6Ru$: Calculated C 53.35; H 4.71; N 9.82. Measured: C 53.21; H 4.46; N 9.68.

[Ru(terpy)(tbbpy)(im-ph-COOH)][BF$_4$]$_2$ (10). A 80 mg portion (0.101 mmol) of [Ru(terpy)(tbbpy)(OH$_2$)][BF$_4$]$_2$ (**2**) and 75 mg (0.399 mmol) of 4-(1*H*-imidazol-1-yl)benzoic acid were refluxed in 20 mL of methanol for 36 h. Solvent then removed in vacuo, and the resulting brown solid was suspended in 1 M HBF$_4$ (aq.) and stirred for 1 h. The brown solid was then filtered and washed with additional 1 M HBF$_4$ (aq.). Yield: 52 mg, 60%. ^1H NMR (400 MHz, DMSO) δ 13.23 (br, s, 1H), 8.99 (d, 1H), 8.83 (d, J = 8.1 Hz, 2H), 8.78−8.72 (m, 3H), 8.69 (d, J = 6.0 Hz, 1H), 8.28 (t, J = 8.2 Hz, 1H), 8.12 (t, J = 7.8 Hz, 2H), 8.02−7.94 (m, 3H), 7.88−7.82 (m, 4H), 7.62 (d, J = 8.6 Hz, 2H), 7.53 (t, 2H), 7.17 (s, 2H), 6.15 (s, 1H), 1.57 (s, 9H), 1.24 (s, 9H). $^{13}C\{^1H\}$ NMR (126 MHz, DMSO) δ 166.27, 161.11, 160.89, 157.88, 157.12, 156.89, 155.24, 152.72, 151.10, 150.20, 138.45, 138.17, 137.67, 135.15, 131.02, 130.72, 130.18, 128.75, 128.55, 124.68, 124.33, 123.59, 121.74, 121.65, 121.02, 120.68, 35.55, 35.20, 30.30, 29.87. Elemental Analysis for $C_{43}H_{43}B_2F_8N_7O_2Ru$: Calculated C 53.55; H 4.49; N 10.17. Measured: C 53.32; H 4.30; N 10.01.

4-(1*H*-imidazol-1-yl)-*N*-((tetrahydro-2*H*-pyran-2-yl)oxy)-benzamide (11). A 400 mg portion (2.12 mmol) of 4-(1*H*-imidazol-1-yl)benzoic acid was put under a nitrogen atmosphere in a 50 mL round-bottom flask fitted with a reflux condenser. Twenty milliliters of thionyl chloride was then added via syringe. The resulting solution was refluxed for 2 h. Excess thionyl chloride was then blown off through a bubbler filled with aqueous potassium carbonate leaving a colorless solid. Without isolation, the colorless solid was dissolved in 5 mL of dry dichloromethane. Separately, 268 mg (2.30 mmol) of *O*-(tetrahydro-2*H*-pyran-2-yl)hydroxylamine was dissolved in 10 mL of dry dichloromethane under nitrogen. Two milliliters of diethylisopropylamine was added to each solution via syringe. The hydroxylamine solution was transferred via cannula to the flask containing the previously generated acid chloride. The reaction solution was stirred at room temperature for 24 h and then washed with aqueous sodium bicarbonate. The organic layer was dried with sodium sulfate and solvent was removed. The product was then purified by alumina chromatography (4% methanol in dichloromethane as eluent) and isolated as a white solid. Yield 225 mg, 37%. ^1H NMR (400 MHz, CD_2Cl_2) δ 7.92−7.88 (m, 2H), 7.87 (s, 1H), 7.48−7.44 (m, 2H), 7.36 (t, J = 1.3 Hz, 1H), 7.17 (s, 1H), 5.08 (s, 1H), 4.05−3.96 (m, 1H), 3.65−3.56 (m, 1H), 1.86−1.78 (m, 3H), 1.71−1.51 (m, 4H). $^{13}C\{^1H\}$ NMR (126 MHz, CD_2Cl_2) δ 164.86, 139.78, 135.70, 131.71, 130.58, 129.65, 120.84, 118.23, 102.75, 62.75, 28.60, 25.43, 19.07. Elemental Analysis for $C_{15}H_{17}N_3O_3$: C 62.17; H 5.96; N 14.63. Measured: C 62.46; H 5.70; N 14.54.

[Ru(terpy)(tbbpy)(im-ph-hydrox)][BF$_4$]$_2$ (12). An 80 mg portion (0.101 mmol) of [Ru(terpy)(tbbpy)(OH$_2$)][BF$_4$]$_2$ (**2**), 75 mg (0.261 mmol) of 4-(1*H*-imidazol-1-yl)-*N*-((tetrahydro-2*H*-pyran-2-yl)oxy)-benzamide, and 40 mg (0.207 mmol) of silver tetrafluoroborate were refluxed in 20 mL of methanol for 48 h in the absence of light. The solution was filtered through Celite, and the solvent was removed. The resulting brown solid was suspended in 1 M HBF$_4$ and stirred for 1 h. The solid was then filtered off and washed with additional 1 M HBF$_4$. Yield: 63 mg, 64%. ^1H NMR (400 MHz, DMSO) δ 9.02−8.97 (m, 1H), 8.83 (dd, J = 8.2, 1.6 Hz, 2H), 8.78−8.72 (m, 3H), 8.67 (dd, J = 14.7, 6.0 Hz, 1H), 8.33−8.25 (m, 1H), 8.12 (t, J = 7.9 Hz, 2H), 8.01−7.92 (m, 2H), 7.88−7.80 (m, 3H), 7.70−7.66 (m, 1H), 7.62−7.57 (m, 1H), 7.56−7.48 (m, 3H), 7.36 (d, J = 9.0 Hz, 1H), 7.17 (s, 2H), 6.11 (d, J = 11.8 Hz, 1H), 3.65 (s, 1H), 1.57 (s, 9H), 1.25 (s, 9H). $^{13}C\{^1H\}$ NMR (126 MHz, DMSO) δ 161.12, 160.90, 157.89, 157.13, 156.90, 155.24, 152.74, 138.18, 135.67, 135.15, 133.55, 130.73, 130.63, 128.86, 128.56, 124.69, 124.32, 123.64, 123.59, 122.05, 121.66, 121.14, 121.03, 120.66, 109.52, 35.56, 35.21, 30.25, 29.88. Carbonyl peak not resolved. HRMS for $(C_{43}H_{43}N_8O_2Ru)^{2+}$ [M-H]$^{2+}$: 402.6276; Calculated: Measured: 402.6325.

Diethyl (4-(1*H*-imidazol-1-yl)phenyl)phosphonate (13). **13** was prepared using a similar method to the analogous compounds.[48] A 222 mg portion (1.00 mmol) of 1-(4-bromophenyl)-1*H*-imidazole and 41 mg of Pd(dppf)Cl$_2$·dichloromethane (5 mol %) were dissolved in 10 mL of dry toluene under nitrogen. A 152 mg portion (1.10 mmol) of diethyl phosphite and 0.15 μL of triethylamine were added via syringe. The resulting solution was stirred at 90 °C for 24 h. The crude reaction was cooled, filtered, and solvent was removed from the filtrate. The product was washed through a plug of alumina using 10% methanol in dichloromethane as eluent. Final purification by recrystallization from hot hexanes yielded a white crystalline solid. Yield: 244 mg, 87%. ^1H NMR (400 MHz, CD_2Cl_2) δ 7.94−7.86 (m, 3H), 7.56−7.50 (m, 2H), 7.38 (s, 1H), 7.19 (s, 1H), 4.31−3.95 (m, 4H), 1.32 (q, J = 6.9 Hz, 6H). $^{13}C\{^1H\}$ NMR (126 MHz, CD_2Cl_2) δ 140.75 (d, J = 3.2 Hz), 135.80, 133.97 (d, J = 10.5 Hz), 131.21, 128.21 (d, J = 190.8 Hz), 121.15 (d, J = 15.4 Hz), 118.15, 62.66 (d, J = 5.5 Hz), 16.55 (d, J = 6.3 Hz). $^{31}P\{^1H\}$ NMR (202 MHz, CD_2Cl_2) δ 16.99. Elemental Analysis for $C_{13}H_{17}N_2O_3P$: Calculated: C 55.71; H 6.11; N 10.00. Measured: C 56.04; H 6.26; N 10.05.

[Ru(terpy)(tbbpy)(im-ph-PO(OEt)$_2$)][BF$_4$]$_2$·2.5(CH$_3$OH) (14). A 135 mg portion (0.170 mmol) of [Ru(terpy)(tbbpy)(OH$_2$)][BF$_4$]$_2$ (**2**), 207 mg (0.739 mmol) of diethyl (4-(1*H*-imidazol-1-yl)phenyl)-phosphonate, and 105 mg (0.544 mmol) of silver tetrafluoroborate were refluxed for 48 h in 25 mL of methanol in the absence of light. The solution was filtered through Celite, and the solvent then removed. The resulting red-brown solid was suspended in 1 M HBF$_4$ (aq.) and stirred for 1 h. The solid was filtered off and washed with additional 1 M HBF$_4$. Impurities were removed chromatographically on neutral alumina using 4% methanol in dichloromethane as eluent. The product eluted as an orange band. The sample for elemental analysis was dissolved in methanol, transferred to a vial, and dried to constant weight. Yield: 169 mg, 94%. ^1H NMR (400 MHz, DMSO) δ 8.99 (s, 1H), 8.84 (d, J = 8.1 Hz, 2H), 8.74 (m, 3H), 8.68 (d, J = 6.1 Hz, 1H), 8.28 (t, J = 8.1 Hz, 1H), 8.12 (dd, J = 8.5, 7.3 Hz, 2H), 7.96 (dd, J = 6.1, 1.9 Hz, 1H), 7.84 (m, 4H), 7.78 (m, 2H), 7.64 (dd, J = 8.6, 3.2 Hz, 2H), 7.55−7.50 (m, 2H), 7.17 (s, 2H), 6.15 (s, 1H), 4.04−3.94 (m, 4H), 1.57 (s, 9H), 1.25 (s, 9H), 1.20 (t, J = 7.1 Hz, 6H). $^{13}C\{^1H\}$ NMR (126 MHz, DMSO) δ 161.12, 160.90, 157.90, 157.14, 156.90, 155.26, 152.74, 151.10, 150.23, 138.27 (d, J = 3.7 Hz), 138.19, 137.76, 135.17, 132.82 (d, J = 10.8 Hz), 128.77, 128.57, 128.20 (d, J = 188.3 Hz), 127.45, 124.69, 124.32, 123.59, 121.69, 121.39 (d, J = 15.1 Hz), 121.14, 120.75, 61.90 (d, J = 5.5 Hz), 35.57, 35.22, 30.31, 29.88, 16.13 (d, J = 5.9 Hz). $^{31}P\{^1H\}$ NMR (162 MHz, DMSO) δ 18.56. Elemental Analysis for $C_{46}H_{52}B_2F_8N_7O_3PRu$·2.5$CH_3OH$: Calculated C 51.25; H 5.50; N 8.63. Measured: C 51.61; H 5.51; N 8.10.

[Ru(terpy)(tbbpy)(im-ph-phos)][BF$_4$]$_2$ (15). In a Schlenk flask, 36 mg (0.034 mmol) of [Ru(terpy)(tbbpy)(im-ph-PO(OEt)$_2$][BF$_4$]$_2$ (**14**) was dissolved in 10 mL of dry dichloromethane under nitrogen. A vast excess of bromotrimethylsilane (0.50 mL) was added via syringe. The resulting solution was stirred at room temperature for 18 h. The volatiles were evaporated leaving a red-brown solid. The brown solid was suspended in water, and dried in vacuo. The solid was then washed with dichloromethane and decanted. The product was obtained as a brown solid. Yield: 15 mg, 44%. ^1H NMR (501 MHz, DMSO) δ 9.01−8.98 (d, J = 2.1 Hz, 1H), 8.87−8.83 (d, J = 8.2 Hz, 2H), 8.77−8.72 (d, J = 7.3 Hz, 3H), 8.71−8.67 (d, J = 6.1 Hz, 1H), 8.31−8.26 (t, J = 8.1 Hz, 1H), 8.14−8.09 (td, J = 7.9, 1.5 Hz, 2H), 8.00−7.95 (dd, J = 6.0, 2.0 Hz, 1H), 7.90−7.83 (m, 4H), 7.82−7.79 (m, 2H), 7.74−7.68 (dd, J = 12.4, 8.3 Hz, 2H), 7.58−7.49 (m, 4H), 7.19−7.15 (d, J = 1.3 Hz, 2H), 6.16−6.13 (t, J = 1.5 Hz, 1H), 1.58−1.55 (s, 9H), 1.27−1.24 (s, 9H). $^{13}C\{^1H\}$ NMR (126 MHz, DMSO) δ 161.12, 160.86, 157.87, 157.11, 152.69, 151.02, 148.01, 141.13, 138.15, 137.51, 135.11, 134.87, 132.16, 132.09, 131.83, 131.74, 128.54, 124.66, 124.34, 123.58, 121.66, 121.55, 120.88, 120.77, 120.58, 99.48, 35.54, 35.19, 30.29, 29.85. In this $^{13}C\{^1H\}$ spectrum it is difficult to determine which peaks are coupled to phosphorus. $^{31}P\{^1H\}$ NMR (122 MHz, DMSO) δ 11.10. HRMS for $(C_{42}H_{44}N_7O_3PRu)^{2+}$: Calculated 413.61436; Measured: 413.61310.

4-(4-(1*H*-imidazol-1-yl)phenyl)-3,5-dimethylisoxazole (16). A 990 mg portion (4.46 mmol) of 1-(4-bromophenyl)-1*H*-imidazole, 1.972 g (10.11 mmol) of 4-(4,5-dimethyl-1,3,2-dioxaborolan-2-yl)-3,5-

dx.doi.org/10.1021/ic4010856 | Inorg. Chem. 2013, 52, 6752−6764

dimethylisoxazole, 370 mg (0.320 mmol) of freshly purified $Pd(PPh_3)_4$, and 5.630 g (32.7 mmol) of barium hydroxide were heated at 80 °C for 18 h under nitrogen in 200 mL of 9:1 1,2-dimethoxyethane:water. The solution was cooled to room temperature, washed with 1 M HCl, and extracted into dichloromethane. The aqueous layer was basified with potassium carbonate and extracted with dichloromethane. The combined organic layers were dried over sodium sulfate, filtered, and the solvent of the filtrate removed. The product was purified by alumina chromatography using 1% methanol in dichloromethane as eluent and recovered as a white solid. Yield: 660 mg, 62%. ^{1}H NMR (400 MHz, CD_2Cl_2) δ 7.90−7.84 (m, 1H), 7.53−7.46 (m, 2H), 7.42−7.37 (m, 2H), 7.36 (t, J = 1.3 Hz, 1H), 7.19−7.14 (m, 1H), 2.42 (s, 3H), 2.27 (s, 3H). ^{13}C{^{1}H} NMR (126 MHz, CD_2Cl_2) δ 165.94, 158.85, 137.06, 135.90, 130.93, 130.85, 130.22, 122.05, 118.49, 115.99, 11.80, 10.96. Elemental Analysis for $C_{14}H_{13}N_3O$: Calculated: C 70.28; H 5.48; N 17.56. Measured: C 70.43; H 5.39; N 17.55.

3-(4-(1*H*-imidazol-1-yl)phenyl)-2,4-pentanedione (17). A 129 mg portion (0.540 mmol) of 4-(4-(1*H*-imidazol-1-yl)phenyl)-3,5-dimethylisoxazole and 86 mg (0.325 mmol) of $Mo(CO)_6$ were *vigorously* refluxed in 20 mL of 1:1 acetonitrile:water for 4 h. Solvent was removed in vacuo. Without further purification, the solid was redissolved in 20 mL of 1:1 ethanol:water and 706 mg (7.75 mmol) of oxalic acid was added. The mixture was stirred at 50 °C for 3 h, after which solvent was removed. The mixture was basified using aqueous sodium bicarbonate and extracted with dichloromethane. The organic fraction was dried using sodium sulfate and solvent removed. The product was isolated by recrystallization from hexanes as a white crystalline solid and stored in the freezer. Yield: 52 mg, 45%. ^{1}H NMR (400 MHz, CD_2Cl_2) δ 16.75 (s, 1H), 7.90−7.87 (m, 1H), 7.48−7.43 (m, 2H), 7.36 (t, J = 1.3 Hz, 1H), 7.35−7.29 (m, 2H), 7.18−7.15 (m, 1H), 1.91 (s, 6H). ^{13}C{^{1}H} NMR (126 MHz, CD_2Cl_2) δ 191.36, 137.09, 136.55, 135.86, 133.06, 130.75, 121.98, 118.45, 114.47, 24.37. Elemental Analysis for $C_{14}H_{13}N_3O$: Calculated: C 69.41; H 5.82; N 11.56. Measured: C 69.34; H 5.91; N 11.72.

Solution UV/vis Absorbance and Emission Spectroscopy. Complexes were dissolved in ethanol to a concentration of 0.1 mM. UV/vis absorbance spectra were recorded on a Varian Cary 3 spectrophotometer. Emission spectra were recorded on an Horiba Fluorolog 3 Time Domain Spectrofluorometer in steady-state mode. The spectrofluorometer was equipped with a xenon lamp coupled to a monochromator set to 475 nm.

Cyclic Voltammetry. Cyclic voltammograms were measured using a three-electrode setup containing a platinum disc working electrode, platinum wire counterelectrode, and BASi Double Junction Reference Electrode (MF-2030) containing a silver wire. A supporting electrolyte of 0.1 M NBu_4BF_4 was used, with 0.3 mM concentrations of the complex of interest in 4 mL of acetonitrile. All measurements were made relative to the Fc^+/Fc redox couple ($E_{1/2}$ = 630 mV vs NHE).

Diffuse Reflectance UV/vis Preparation and Procedure. TiO_2 thin films were prepared on 25 mm × 25 mm glass coverslips by spin coating a solution of TiO_2 nanoparticles (P25, Degussa) (1 g in 4 mL 50/50 (v/v) ethanol/deionized water) using a Headway PWM32 Spin Coater (Headway Research Inc.). The films were sintered at 450 °C for 2 h with a ramp rate of 5 °C/min, and the resulting total film thickness was 3.5 μm.[39]

The desired dye was dissolved in ethanol (0.3 mM solution), and spin-coated slides were submerged in the dye solution in the absence of light for 36 h. Slides were then washed with excess ethanol to remove any unbound dye. UV/vis spectra were recorded using a Varian Cary 3E spectrophotometer operating in diffuse reflectance mode.

Solar Cell Preparation and Measurement. DSSCs were prepared by spin coating a solution of TiO_2 nanoparticles (P25, Degussa) (1 g in 4 mL 1:1 ethanol/deionized water) using a Headway PWM32 Spin Coater (Headway Research Inc.). Glass coated with fluorine-doped tin oxide (TEC 7, Hartford Glass Inc., U.S.A.) was rinsed thoroughly with ethanol prior to coating, and a spin speed of 1000 rpm was used to yield a 3.5-μm thick film.[39] A subsequent layer was deposited yielding a total thickness of 7 μm. After drying at room temperature, a 0.25 cm^2 template was used to cut out the DSSC active areas. Excess TiO_2 was scraped off, and the working electrodes were cleaned with ethanol before sintering in air at 450 °C for 2 h with a ramp rate of 5 °C/min. The TiO_2 electrodes were then immersed in dye solutions as described above for 36 h.

Prior to DSSC assembly, the electrodes were removed from dye solution and rinsed thoroughly with absolute ethanol. Platinum counter electrodes and iodide/triiodide redox electrolyte were prepared by methods outlined previously.[41] Solar cells were assembled prior to testing using a 60-μm plastic thermal spacer (SX1170−60, Solaronix SA, Switzerland) between electrodes and were held together with metal binder clips. Photocurrent−voltage measurements were performed using a 300 W ozone-free xenon lamp with an AM 1.5G filter (Newport, U.S.A.) as a light source and were recorded using a Keithley 2400 digital source meter. The light intensity of the AM 1.5G filtered xenon lamp was adjusted to 100 mW/cm^2 prior to testing. Exact solar cell surface areas were confirmed by scanning the working electrodes with a 1200 dpi scanner.

■ ASSOCIATED CONTENT

Ⓢ Supporting Information

Selected ^{1}H NMR spectra, emission spectra, cyclic voltammograms. This material is available free of charge via the Internet at http://pubs.acs.org.

■ AUTHOR INFORMATION

Corresponding Author

*E-mail: robert.crabtree@yale.edu (R.H.C.), victor.batista@yale.edu (V.S.B.), charles.schmuttenmaer@yale.edu (C.A.S.), steven.konezny@yale.edu (S.J.K.).

Present Address

†Department of Chemistry, Box 351700, University of Washington, Seattle, Washington 98195-1700.

Author Contributions

The manuscript was written through contributions of all authors. All authors have given approval to the final version of the manuscript.

Notes

The authors declare no competing financial interest.

■ ACKNOWLEDGMENTS

The authors thank Oana Luca and Alexandra Schatz for assistance with electrochemical measurements. T.P.B. thanks Wilson Bailey for editorial assistance. The authors all specially thank the Yale Green Energy Consortium for helpful discussion and feedback. This material is based in part upon work supported as part of the Argonne-Northwestern Solar Energy Research (ANSER) Center, an Energy Frontier Research Center funded by the U.S. Department of Energy, Office of Science, Office of Basic Energy Sciences under Award Number DE-PS02-08ER15944 (T.P.B., L.A.M. solar cells, R.H.C., and V.S.B), by U.S. DoE Award 1043588 (T.P.B. synthesis), and by an NSF Graduate Research Fellowship (S.W.S. solar cells). V.S.B. acknowledges supercomputing time from NERSC.

■ REFERENCES

(1) Lewis, N. S.; Nocera, D. G. *Proc. Natl. Acad. Sci. U.S.A.* **2006**, *103*, 15729.
(2) Lewis, N. S. *Science* **2007**, *315*, 798.
(3) Grätzel, M. *Nature* **2001**, *414*, 338.
(4) Grätzel, M. *J. Photochem. Photobiol. C* **2003**, *4*, 145.
(5) O'Regan, B.; Grätzel, M. *Nature* **1991**, *353*, 737.
(6) Nazeeruddin, M. K.; Kay, A.; Rodicio, I.; Humphry-Baker, R.; Muller, E.; Liska, P.; Vlachopoulos, N.; Grätzel, M. *J. Am. Chem. Soc.* **1993**, *115*, 6382.

(7) Bomben, P. G.; Robson, K. C. D.; Koivisto, B. D.; Berlinguette, C. P. *Coord. Chem. Rev.* **2012**, *256*, 1438.
(8) Han, L.; Islam, A.; Chen, H.; Malapaka, C.; Chiranjeevi, B.; Zhang, S.; Yang, X.; Yanagida, M. *Energy Env. Sci.* **2012**, *5*, 6057.
(9) Chen, C.-Y.; Wang, M.; Li, J.-Y.; Pootrakulchote, N.; Alibabaei, L.; Ngoc-le, C.-H.; Decoppet, J.-D.; Tsai, J.-H.; Grätzel, C.; Wu, C.-G.; Zakeeruddin, S. M.; Grätzel, M. *ACS Nano* **2009**, *3*, 3103.
(10) Fujishima, A.; Honda, K. *Nature* **1972**, *238*, 37.
(11) Vougioukalakis, G. C.; Philippopoulos, A. I.; Stergiopoulos, T.; Falaras, P. *Coord. Chem. Rev.* **2011**, *255*, 2602.
(12) Nazeeruddin, M. K.; Pechy, P.; Renouard, T.; Zakeeruddin, S. M.; Humphry-Baker, R.; Comte, P.; Liska, P.; Cevey, L.; Costa, E.; Shklover, V.; Spiccia, L.; Deacon, G. B.; Bignozzi, C. A.; Grätzel, M. *J. Am. Chem. Soc.* **2001**, *123*, 1613.
(13) Nazeeruddin, M. K.; De Angelis, F.; Fantacci, S.; Selloni, A.; Viscardi, G.; Liska, P.; Ito, S.; Bessho, T.; Grätzel, M. *J. Am. Chem. Soc.* **2005**, *127*, 16835.
(14) Hagfeldt, A.; Boschloo, G.; Sun, L. C.; Kloo, L.; Pettersson, H. *Chem. Rev.* **2010**, *110*, 6595.
(15) Young, K. J.; Martini, L. A.; Milot, R. L.; Snoeberger, R. C., III; Batista, V. S.; Schmuttenmaer, C. A.; Crabtree, R. H.; Brudvig, G. W. *Coord. Chem. Rev.* **2012**, *256*, 2503.
(16) Hanson, K.; Brennaman, M. K.; Luo, H.; Glasson, C. R. K.; Concepcion, J. J.; Song, W.; Meyer, T. J. *ACS Appl. Mater. Interfaces* **2012**, *4*, 1462.
(17) Youngblood, W. J.; Lee, S.-H. A.; Maeda, K.; Mallouk, T. E. *Acc. Chem. Res.* **2009**, *42*, 1966.
(18) Li, L.; Duan, L. L.; Xu, Y. H.; Gorlov, M.; Hagfeldt, A.; Sun, L. C. *Chem. Commun.* **2010**, *46*, 7307.
(19) Youngblood, W. J.; Lee, S.-H. A.; Kobayashi, Y.; Hernandez-Pagan, E. A.; Hoertz, P. G.; Moore, T. A.; Moore, A. L.; Gust, D.; Mallouk, T. E. *J. Am. Chem. Soc.* **2009**, *131*, 926.
(20) Brimblecombe, R.; Koo, A.; Dismukes, G. C.; Swiegers, G. F.; Spiccia, L. *J. Am. Chem. Soc.* **2010**, *132*, 2892.
(21) Duan, L.; Tong, L.; Xu, Y.; Sun, L. *Energy Env. Sci.* **2011**, *4*, 3296.
(22) Gao, Y.; Ding, X.; Liu, J.; Wang, L.; Lu, Z.; Li, L.; Sun, L. *J. Am. Chem. Soc.* **2013**, *135*, 4219.
(23) Gillaizeau-Gauthier, I.; Odobel, F.; Alebbi, M.; Argazzi, R.; Costa, E.; Bignozzi, C. A.; Qu, P.; Meyer, G. J. *Inorg. Chem.* **2001**, *40*, 6073.
(24) Bae, E.; Choi, W. *J. Phys. Chem. B* **2006**, *110*, 14792.
(25) McNamara, W. R.; Milot, R. L.; Song, H. E.; Snoeberger, R. C.; Batista, V. S.; Schmuttenmaer, C. A.; Brudvig, G. W.; Crabtree, R. H. *Energy Env. Sci.* **2010**, *3*, 917.
(26) McNamara, W. R.; Snoeberger, R. C.; Li, G. H.; Richter, C.; Allen, L. J.; Milot, R. L.; Schmuttenmaer, C. A.; Crabtree, R. H.; Brudvig, G. W.; Batista, V. S. *Energy Env. Sci.* **2009**, *2*, 1173.
(27) Yang, J.; Bremer, P. J.; Lamont, I. L.; McQuillan, A. J. *Langmuir* **2006**, *22*, 10109.
(28) Moser, J.; Punchihewa, S.; Infelta, P. P.; Graetzel, M. *Langmuir* **1991**, *7*, 3012.
(29) Abuabara, S. G.; Cady, C. W.; Baxter, J. B.; Schmuttenmaer, C. A.; Crabtree, R. H.; Brudvig, G. W.; Batista, V. S. *J. Phys. Chem. C* **2007**, *111*, 11982.
(30) McNamara, W. R.; Snoeberger, R. C.; Li, G.; Schleicher, J. M.; Cady, C. W.; Poyatos, M.; Schmuttenmaer, C. A.; Crabtree, R. H.; Brudvig, G. W.; Batista, V. S. *J. Am. Chem. Soc.* **2008**, *130*, 14329.
(31) Olivier, J.-H.; Haefele, A.; Retailleau, P.; Ziessel, R. *Org. Lett.* **2009**, *12*, 408.
(32) Xiao, D.; Martini, L. A.; Snoeberger, R. C.; Crabtree, R. H.; Batista, V. S. *J. Am. Chem. Soc.* **2011**, *133*, 9014.
(33) Heimer, T. A.; D'Arcangelis, S. T.; Farzad, F.; Stipkala, J. M.; Meyer, G. J. *Inorg. Chem.* **1996**, *35*, 5319.
(34) Ernstorfer, R.; Gundlach, L.; Felber, S.; Storck, W.; Eichberger, R.; Willig, F. *J. Phys. Chem. B* **2006**, *110*, 25383.
(35) Nilsing, M.; Persson, P.; Ojamae, L. *Chem. Phys. Lett.* **2005**, *415*, 375.
(36) Hanson, K.; Brennaman, M. K.; Ito, A.; Luo, H. L.; Song, W. J.; Parker, K. A.; Ghosh, R.; Norris, M. R.; Glasson, C. R. K.; Concepcion, J. J.; Lopez, R.; Meyer, T. J. *J. Phys. Chem. C* **2012**, *116*, 14837.
(37) Park, H.; Bae, E.; Lee, J.-J.; Park, J.; Choi, W. *J. Phys. Chem. B* **2006**, *110*, 8740.
(38) Brown, D. G.; Schauer, P. A.; Borau-Garcia, J.; Fancy, B. R.; Berlinguette, C. P. *J. Am. Chem. Soc.* **2013**, *135* (5), 1692.
(39) Martini, L. A.; Moore, G. F.; Milot, R. L.; Cai, L. Z.; Sheehan, S. W.; Schmuttenmaer, C. A.; Brudvig, G. W.; Crabtree, R. H., submitted for publication.
(40) Mollmann, U.; Heinisch, L.; Bauernfeind, A.; Kohler, T.; Ankel-Fuchs, D. *Biometals* **2009**, *22*, 615.
(41) Moore, G. F.; Konezny, S. J.; Song, H. E.; Milot, R. L.; Blakemore, J. D.; Lee, M. L.; Batista, V. S.; Schmuttenmaer, C. A.; Crabtree, R. H.; Brudvig, G. W. *J. Phys. Chem. C* **2012**, *116*, 4892.
(42) Brewster, T. P.; Ding, W. D.; Schley, N. D.; Hazari, N.; Batista, V. S.; Crabtree, R. H. *Inorg. Chem.* **2011**, *50*, 11938.
(43) Yavin, E.; Weiner, L.; Arad-Yellin, R.; Shanzer, A. *J. Phys. Chem. A* **2001**, *105*, 8018.
(44) Demmer, C. S.; Krogsgaard-Larsen, N.; Bunch, L. *Chem. Rev.* **2011**, *111*, 7981.
(45) Zhang, Y.; Chen, B.; Fronczek, F. R.; Maverick, A. W. *Inorg. Chem.* **2008**, *47*, 4433.
(46) Labadie, S. S. *Synth. Commun.* **1994**, *24*, 709.
(47) Sazanovich, I. V.; Balakumar, A.; Muthukumaran, K.; Hindin, E.; Kirmaier, C.; Diers, J. R.; Lindsey, J. S.; Bocian, D. F.; Holten, D. *Inorg. Chem.* **2003**, *42*, 6616.
(48) Spampinato, V.; Tuccitto, N.; Quici, S.; Calabrese, V.; Marletta, G.; Torrisi, A.; Licciardello, A. *Langmuir* **2010**, *26*, 8400.
(49) Pechy, P.; Rotzinger, F. P.; Nazeeruddin, M. K.; Kohle, O.; Zakeeruddin, S. M.; Humphry-Baker, R.; Grätzel, M. *J. Chem. Soc. Chem. Comm* **1995**, 65.
(50) Sze, S. M. *Physics of Semiconductor Devices.*; John Wiley & Sons: New York, 1981.
(51) Dongaonkar, S.; Servaites, J. D.; Ford, G. M.; Loser, S.; Moore, J.; Gelfand, R. M.; Mohseni, H.; Hillhouse, H. W.; Agrawal, R.; Ratner, M. A.; Marks, T. J.; Lundstrom, M. S.; Alam, M. A. *J. Appl. Phys.* **2010**, *108*, 124509.
(52) Halme, J.; Vahermaa, P.; Miettunen, K.; Lund, P. *Adv. Mater.* **2010**, *22*, E210.
(53) Schlichthörl, G.; Huang, S. Y.; Sprague, J.; Frank, A. J. *J. Phys. Chem. B* **1997**, *101*, 8141.
(54) Boschloo, G.; Haggman, L.; Hagfeldt, A. *J. Phys. Chem. B* **2006**, *110*, 13144.
(55) Koops, S. E.; O'Regan, B. C.; Barnes, P. R. F.; Durrant, J. R. *J. Am. Chem. Soc.* **2009**, *131*, 4808.
(56) Zhang, K.; Zhang, S.; Sodeyama, K.; Yang, X.; Chen, H.; Yanagida, M.; Tateyama, Y.; Han, L. *Appl. Phys. Express* **2012**, *5*, 042303.
(57) Kroon, J. M.; Bakker, N. J.; Smit, H. J. P.; Liska, P.; Thampi, K. R.; Wang, P.; Zakeeruddin, S. M.; Grätzel, M.; Hinsch, A.; Hore, S.; Wurfel, U.; Sastrawan, R.; Durrant, J. R.; Palomares, E.; Pettersson, H.; Gruszecki, T.; Walter, J.; Skupien, K.; Tulloch, G. E. *Prog. Photovoltaics* **2007**, *15*, 1.
(58) Sullivan, B. P.; Calvert, J. M.; Meyer, T. J. *Inorg. Chem.* **1980**, *19*, 1404.
(59) Pangborn, A. B.; Giardello, M. A.; Grubbs, R. H.; Rosen, R. K.; Timmers, F. J. *Organometallics* **1996**, *15*, 1518.

Supporting Information for

Hydroxamate Anchors for Improved Photoconversion in Dye-Sensitized Solar Cells

Timothy P. Brewster,† Steven J. Konezny, Lauren A. Martini, Stafford W. Sheehan, Charles A. Schmuttenmaer,* Victor S. Batista,* Robert H. Crabtree**

Yale University, Department of Chemistry, P.O. Box 208107, New Haven, CT 06520-8107

Energy Sciences Institute, Yale University, P.O. Box 27394, West Haven, CT 06516-7394

† Current address: Department of Chemistry, Box 351700, University of Washington, Seattle, Washington 98195-1700

Email: robert.crabtree@yale.edu, victor.batista@yale.edu, charles.schmuttenmaer@yale.edu, steven.konezny@yale.edu

Table of Contents

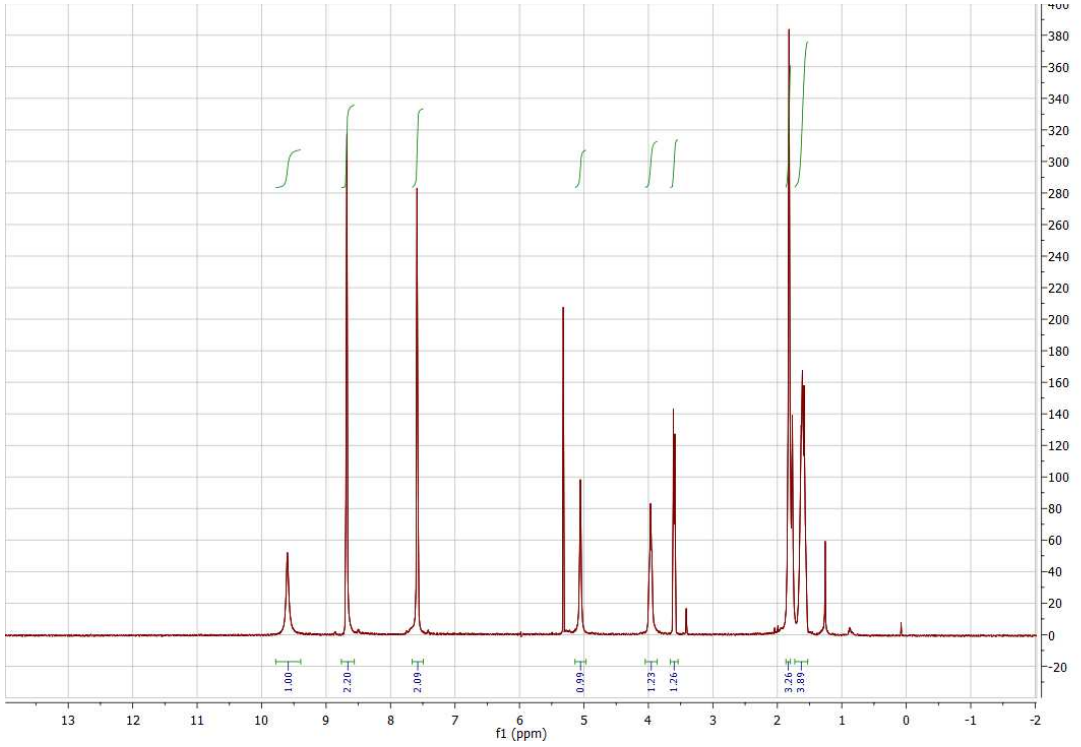

S1. [1]HNMR Spectra of N-((tetrahydro-2H-pyran-2-yl)oxy)isonicotinamide

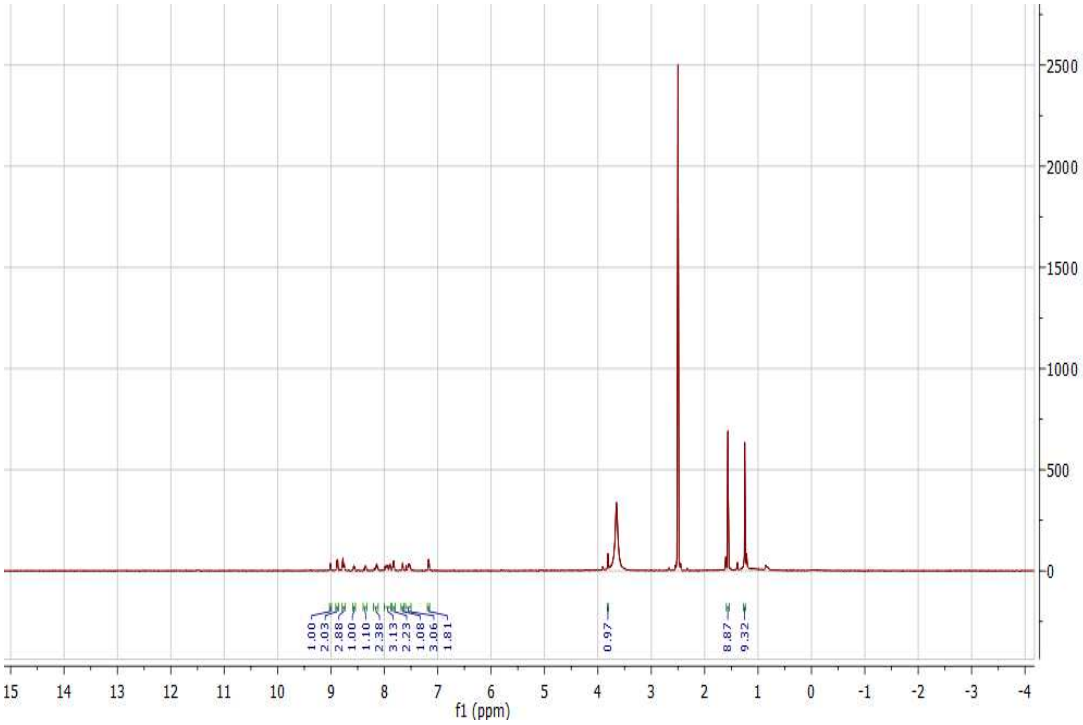

S2. [1]HNMR Spectra of $[Ru(terpy)(tbbpy)(pyr\text{-}hydrox)][BF_4]_2$ (**4**)

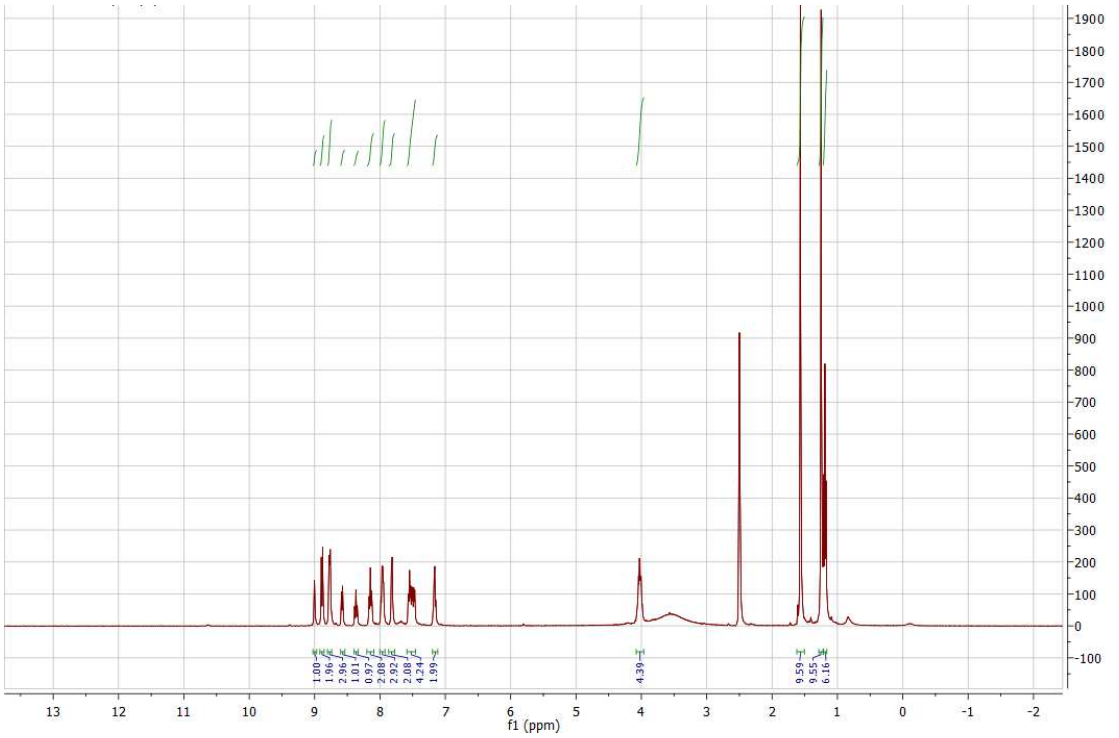

S3. ^{1}HNMR Spectra of [Ru(terpy)(tbbpy)(pyr-PO(OEt)$_2$)][BF$_4$]$_2$ (**5**)

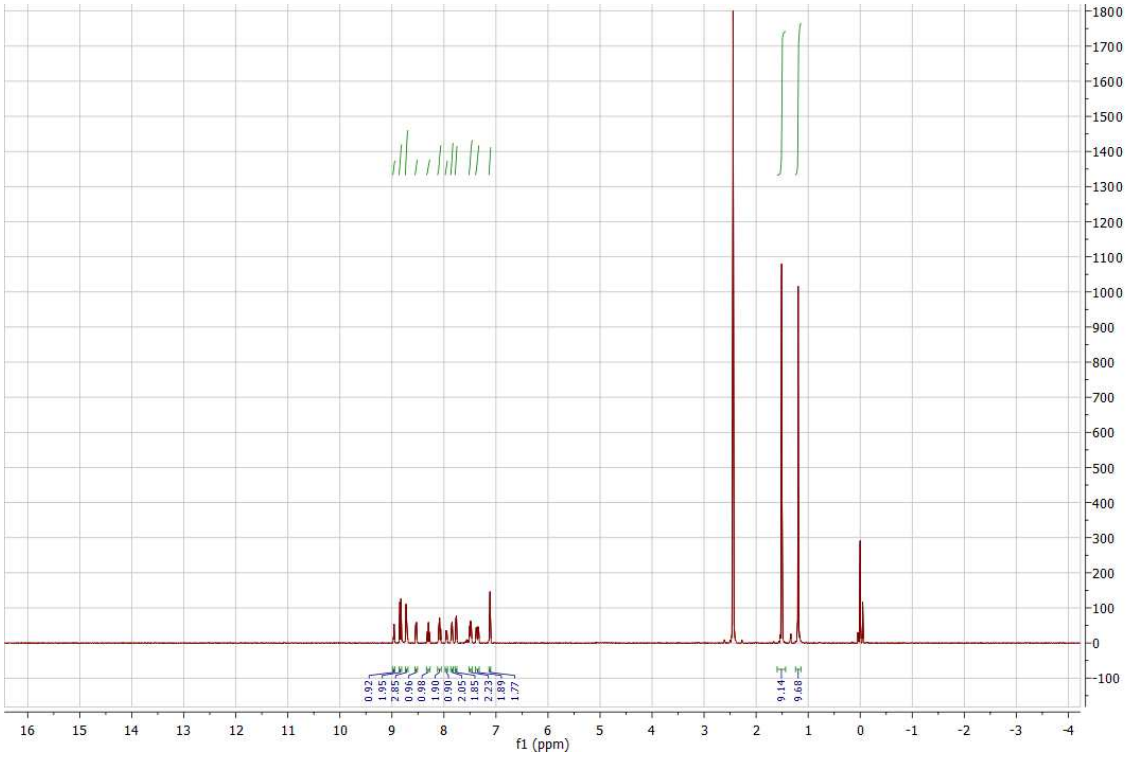

S4. ^{1}HNMR Spectra of [Ru(terpy)(tbbpy)(pyr-phos)][BF$_4$]$_2$ (**6**)

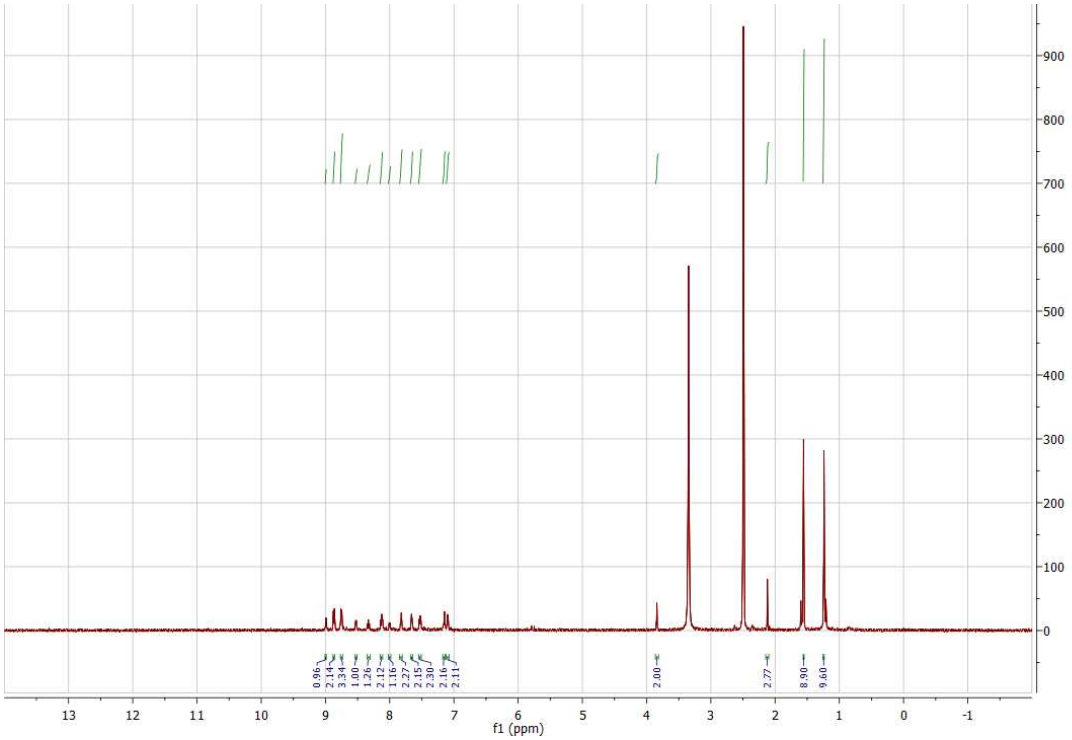

S5. [1]HNMR Spectra of [Ru(terpy)(tbbpy)(pyr-acetone)][BF_4]$_2$ (**8**)

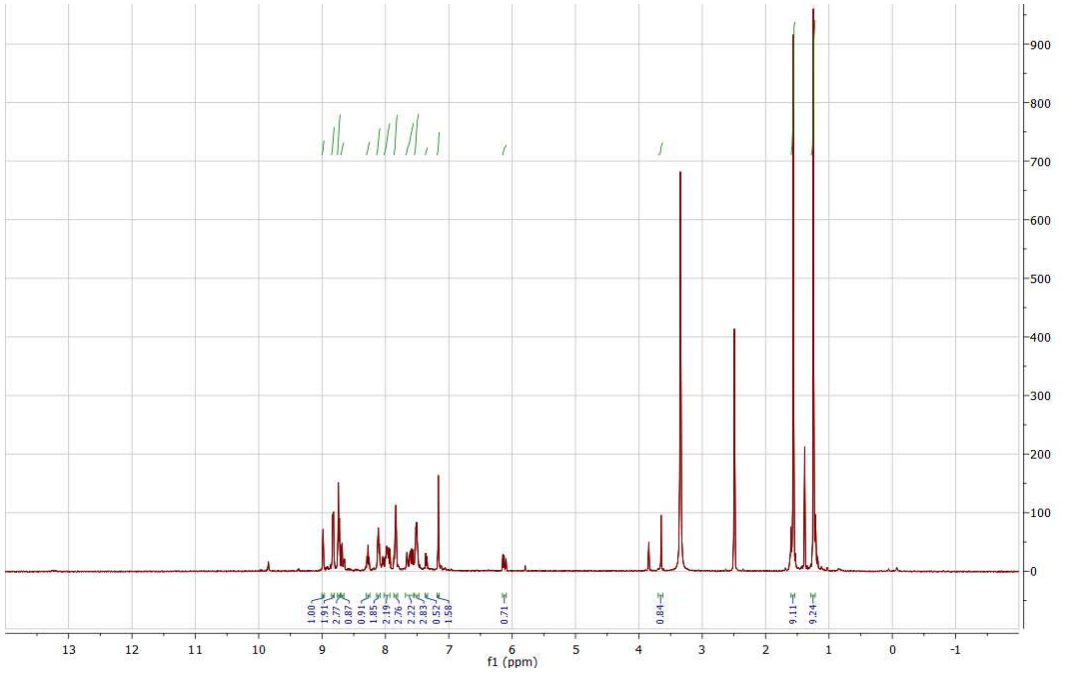

S6. [1]HNMR Spectra of [Ru(terpy)(tbbpy)(im-ph-hydrox)][BF_4]$_2$ (**12**). Extra peaks are water at δ 3.3 and methanol at δ 1.5 and 3.8.

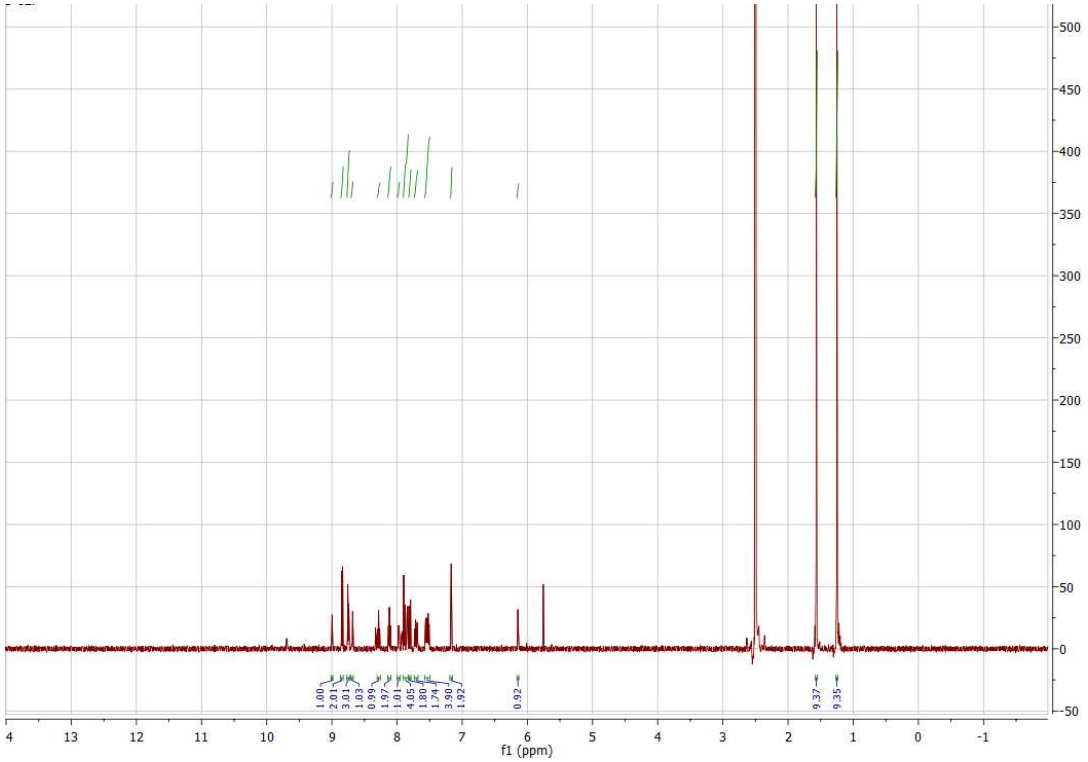

S7. ^{1}HNMR Spectra of $[Ru(terpy)(tbbpy)(im\text{-}ph\text{-}phos)][BF_4]_2$ (**15**). Extra peak at δ 5.7 is dichloromethane.

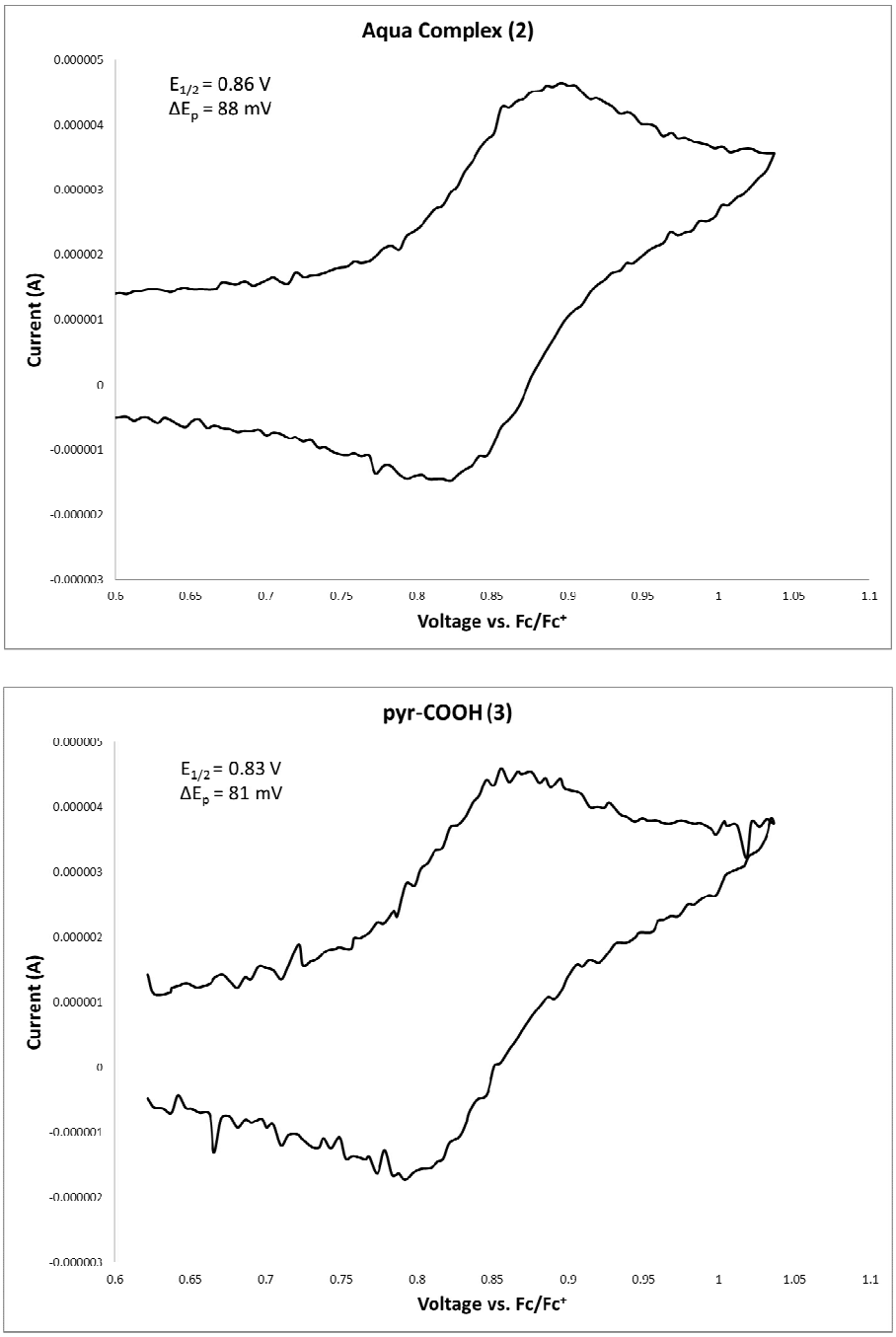

Figure S8. Cyclic Voltammetry of **2** and **3** in 0.3 mM acetonitrile solution using 0.1 M NBu_4BF_4 as supporting electrolyte.

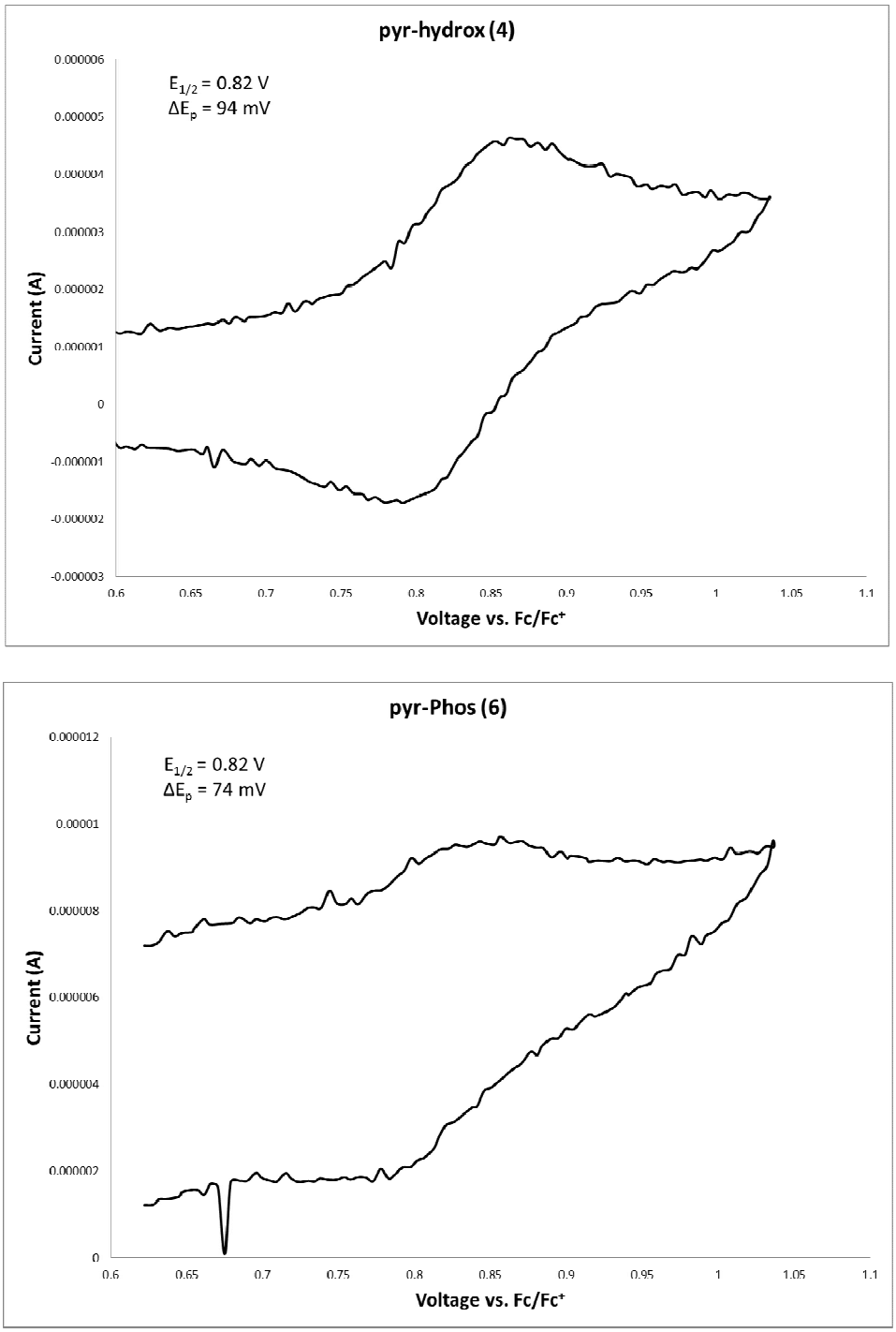

Figure S9. Cyclic Voltammetry of **4** and **6** in 0.3 mM acetonitrile solution using 0.1 M NBu_4BF_4 as supporting electrolyte.

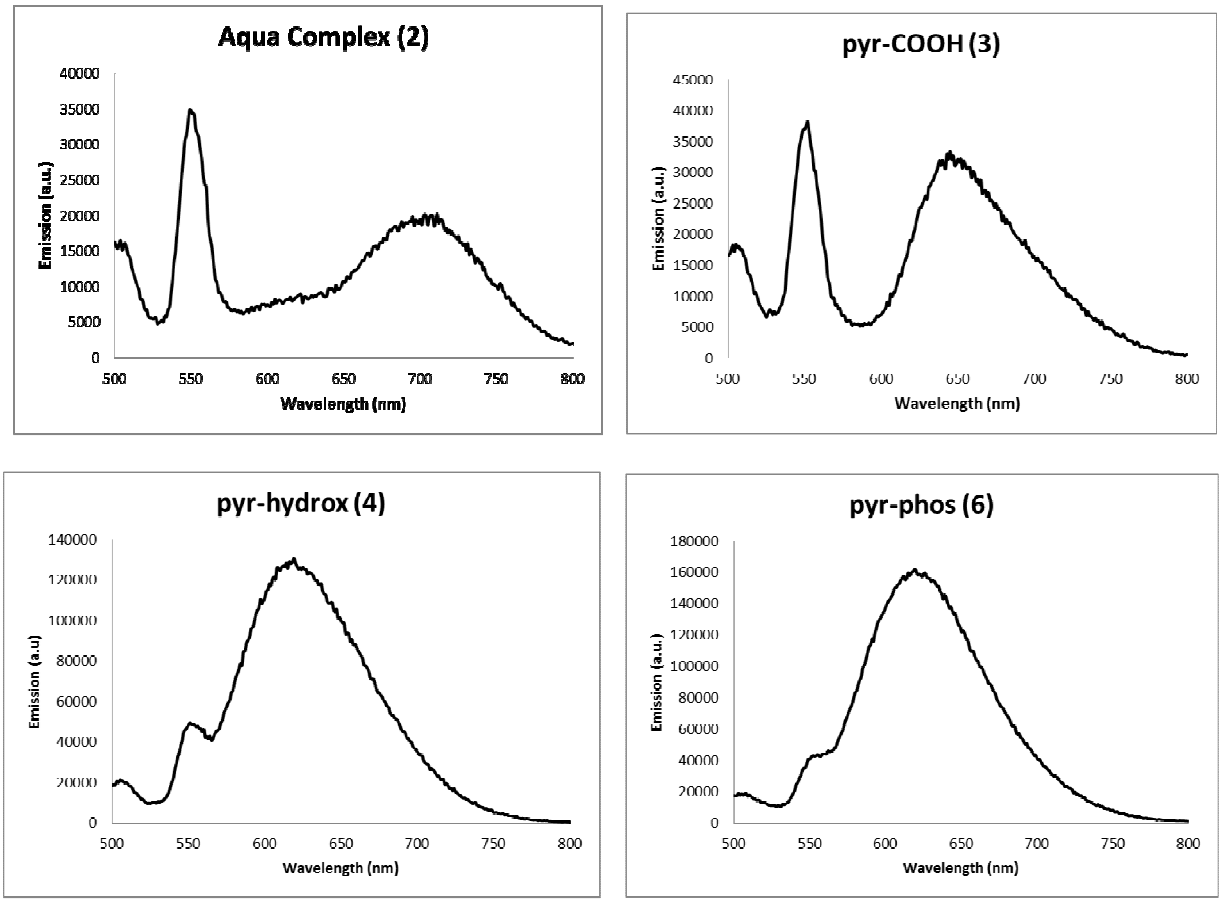

Figure S10. Emission spectra of **2**, **3**, **4**, and **6** as 0.1 mM solutions in ethanol. λ_{max} for the lowest energy features are at 695 nm (**2**), 640 nm (**3**), 619 nm (**4**), and 619 nm (**6**).